

**FABRICATION OF FLEXIBLE MICRO-LENS ARRAY
FOR OPTICAL NEURAL STIMULATION**

By

Xiaopeng Bi

A THESIS

Submitted to
Michigan State University
in partial fulfillment of the requirements
for the degree of

Electrical Engineering—Master of Science

2014

ABSTRACT

FABRICATION OF FLEXIBLE MICRO-LENS ARRAY FOR OPTICAL NEURAL STIMULATION

By

Xiaopeng Bi

Optogenetics is a fast growing neuromodulation technique which can remotely manipulate the specific activities of targeted neurons with irradiation of light. It benefits exploration of neuron network dynamics and also clinical studies such as retinal prosthesis. Light emitting diode (LED) offers a great option as the light source for optogenetics because it is small, reliable and easy to control. Especially, arrays of LEDs have been developed to enable multisite stimulation. A major drawback of LED is its intrinsically low out-coupling efficiency of light as a result of a large emitting angle around 90° to 120° . In this thesis, the employment of μ -lens array has been proposed to couple with LED and target the improvement of light out-coupling efficiency, which will lead to a higher spatial resolution for optical neural stimulation. A number of techniques, including surface tension modification, soft lithography, thermal reflow, and self-organized dewetting, have been studied to fabricate the array of μ -lenses on a flexible polymer substrate. Surface morphology of such μ -lens array has been analyzed both experimentally and theoretically. Experiment in the medium of gelatin has been carried out to mimic the light irradiation property in the natural tissue.

ACKNOWLEDGMENTS

I would like to gratefully thank my advisor Prof. Wen Li for her continuing guidance and support during my master study. Her expertise, insight and advice are precious to me and very helpful to keep my research progressing on the right track. Special thanks to her kindness, patience and understanding.

I am also highly indebted to my thesis committee, including Prof. Lixin Dong, Prof. Andrew J. Mason and Prof. Ilsoon Lee for their constructive suggestions and insightful comments regarding my research over the years.

I would also like to express my gratitude to my colleagues Brian Crum, Bin Fan, Nathan Wood, Ki Yong Kwon, Haider Al-Mumen, Lin Li and Yue Huang for their technical assistance, as well as my friends for their supportive encouragement which is invaluable to me.

Finally, and most importantly, I would like to sincerely thank my wife Rui Xu and my parents for their consistent support, encouragement and unending love throughout the time of my graduate study and my life. This work is dedicated to them.

TABLE OF CONTENTS

LIST OF FIGURES	vi
CHAPTER 1 Introduction	1
1.1 Motivation.....	1
1.1.1 Optogenetics	1
1.1.2 Light sources for optogenetics.....	3
1.2 Objective.....	5
1.3 Thesis Outline	5
CHAPTER 2 Lens Fabrication through Soft Lithography	7
2.1 Background.....	7
2.2 Lens Design	8
2.2.1 Property of LED.....	8
2.2.2 Optical path design	8
2.2.3 Simulation	10
2.3 Lens Fabrication.....	11
2.3.1 Material	11
2.3.2 Fabrication process	12
2.3.3 Device assembly	14
2.4 Measurement.....	14
2.5 Summary	16
CHAPTER 3 Surface Tension Modification by Plasma Treatment	17
3.1 Background.....	17
3.2 Experiment.....	18
3.2.1 Material	18
3.2.2 Process	19
3.2.3 Measurement.....	20
3.3 Results.....	20
3.3.1 Static WCA measurements	20
3.3.2 Surface roughness	22
3.3.3 Surface chemistry.....	23
3.3.4 Switchability	25
3.4 Analysis.....	26
3.5 Summary	31
CHAPTER 4 Fabrication of Micro-lens Array through Thermal Reflow	33
4.1 Background.....	33
4.2 Experiment.....	34
4.3 Results and Analysis	35
4.3.1 Microscopic view.....	35
4.3.2 Profile.....	37

4.3.3	SEM images	40
4	Summary	42
CHAPTER 5 Fabrication of Micro-lens Array through Dewetting.....		43
5.1	Background.....	43
5.2	Experiment.....	43
5.2.1	Dewetting of SU-8 on PDMS	43
5.2.2	Room-temperature dewetting exploration	46
5.2.3	Dewetting of SU-8 on Parylene-C	47
5.3	Summary	48
CHAPTER 6 Summary.....		49
REFERENCES		51

LIST OF FIGURES

Figure 1	Principle of electrical stimulation and optogenetics [5].	1
Figure 2	The realization of optogenetics [9].	2
Figure 3	Conceptual diagram of the 3-D multi-waveguide probe array [16].	4
Figure 4	Commercialized macro-scale LED lenses, which are often comprised of a central spherical lens and a cone-shaped reflecting sidewall [23].	7
Figure 5	The LED used in the experiment. It is packaged with a colorless diffused resin.	8
Figure 6	Irradiation characteristic of the LED used in the experiment.	9
Figure 7	The designed LED lens, which is comprised of a central lens and a reflecting sidewall, in order to collimate the LED light and improve the out-coupling efficiency.	9
Figure 8	The radiant intensity as a function of light emitting angle of LED, with various curvature of central lens, with different thickness t .	10
Figure 9	Irradiance map of incident flux on the surface located at 5 mm away from the LED (a) without the lens and (b) with the optimized lens.	11
Figure 10	Process flow for lens fabrication.	12
Figure 11	(a) Lenses fabricated by soft lithography; (b) LEDs and Lenses assembled on the polyimide substrate patterned with circuit.	14
Figure 12	Measurement of light intensity emitted from LEDs with and without coupled lenses. The distribution of light rays clearly shows the converging effect.	15
Figure 13	Blue light distribution along the normal direction of the device.	16
Figure 14	WCAs and RMS surface roughness on O_2 and SF_6 plasma-treated Parylene-C thin films as a function of the O_2 plasma pre-treatment time.	21
Figure 15	The representative 3-D images of Parylene-C surfaces and corresponding WCA images, with (a) no treatment, and plasma-treated with (b) 1 min O_2 + 1 min SF_6 , (c) 5 min O_2 + 1 min SF_6 , and (d) 10 min O_2 + 1 min SF_6 .	22
Figure 16	The representative XPS survey spectra and corresponding fitted high-resolution C1s spectra (inlets) of Parylene-C surfaces with (a) no treatment, and plasma-treated with (b) 10 min O_2 and (c) 10 min O_2 + 1 min SF_6 . The peaks are labeled with corresponding elements in survey spectra and carbon-related functional groups in high-resolution C1s spectra.	24

Figure 17	The switchability between super hydrophobicity and super hydrophilicity on Parylene-C thin films. The original point corresponds to the Parylene-C surface plasma-treated by 10 min O ₂ + 1 min SF ₆ . Afterward, O ₂ and SF ₆ plasma treatments were alternately conducted for 1 min each on the same sample.26
Figure 18	The advancing, receding and static WCAs on COS-treated Parylene-C thin films as a function of the O ₂ plasma pre-treatment time. The insets show the representative WCA images on Parylene-C surfaces plasma-treated with 5 min O ₂ + 1 min SF ₆ (left) and 10 min O ₂ + 1 min SF ₆ (right), which correspond to the water droplets in the Wenzel state and Cassie state, respectively.29
Figure 19	The predictive surface free energies (SFEs, γ_s) on COS-treated Parylene-C thin films as a function of the O ₂ plasma pre-treatment time.30
Figure 20	The value of minus cosine of the static WCA and WCA hysteresis on COS-treated Parylene-C surfaces as a function of the surface roughness factor r . The points also correspond to the various pre-treatment time by O ₂ plasma from 0 (leftmost), 20 s, 40 s, 1 min, 2 min to 10 min (rightmost). The diamond point represents the extrapolated value on a theoretical ideally flat ($r = 1$) Parylene-C surface, which is chemically the same as the surface treated by O ₂ and SF ₆ plasmas. Two regions are distinguished by the dashed line on both curves, implying a transition of droplet status from the Wenzel state to the Cassie state.31
Figure 21	The evolution of the cross-section of photoresist structures during the reflow process, as the baking temperature increases [60].33
Figure 22	The reported μ -lens array with lens diameter of 80 μm fabricated through thermal reflow [61].34
Figure 23	Schematic illustration of the formation of μ -lens array produced by photoresist thermal reflow technique: (a) AZ4620 was spin-coated on the substrate; (b) photoresist cylinders were obtained after photolithography; (c) during the reflow, the profile of patterned photoresist was changed into spherical lens-shape due to the surface tension effect.35
Figure 24	Microscopic view of AZ4620 micro-patterns (a)-(c) before and (d)-(f) after reflow on the silicon substrate. The diameters are (a) (d) 200 μm , (b) (e) 300 μm , and (c) (f) 400 μm , respectively.36
Figure 25	The profile of micro-patterns with various initial diameters of (a) 200 μm , (b) 300 μm and (c) 400 μm on silicon substrates during thermal reflow. (a) and (b) spherical lens-shape was finally achieved; (c) hollows still existed on the top middle.38
Figure 26	The final profile of μ -lenses with various initial diameters of (a) 200 μm , (b) 300 μm and (c) 400 μm on PDMS substrates after thermal reflow at 160 $^{\circ}\text{C}$ lasting for 3 days.39

Figure 27	Contact angles of μ -lenses on silicon and PDMS substrates. The lenses were made by AZ4620 through thermal reflow process with 160 °C lasting for 3 days.	40
Figure 28	SEM images of fabricated μ -lens array and single μ -lens with an initial diameter of 200 μ m on (a) silicon, (b) PDMS, and (c) Parylene-C substrates. Such μ -lens array was made by photoresist AZ4620 and achieved through the thermal reflow technique.	41
Figure 29	Process flow of SU-8 dewetting process on PDMS substrate.	44
Figure 30	SEM images of (a) μ -lens array and (b) single μ -lens with an initial diameter of 200 μ m after SU-8 dewetting on the PDMS substrate. Such array was self-organized onto the surface area that had been pre-treated by O ₂ plasma.	45
Figure 31	The profile of SU-8 μ -lenses with diameters of (a) 200 μ m, (b) 300 μ m, (c) 400 μ m, and (d) 600 μ m, which were fabricated by dewetting on pre-patterned PDMS substrates.	45
Figure 32	Contact angles of SU-8 μ -lenses with various diameters from 200 μ m to 600 μ m on the O ₂ -plasma-treated PDMS substrate. The μ -lenses were fabricated by dewetting.	46
Figure 33	Microscopic view of the surface of (a) flat SU-8 coating on the Parylene-C substrate before dewetting; (b) SU-8 μ -lens array on the Parylene-C substrate after dewetting.	48

CHAPTER 1 Introduction

1.1 Motivation

1.1.1 Optogenetics

Optogenetics is a fast growing neuromodulation technique which is employed in neuroscience and neurobiology [1-5]. The characteristic of this technique is to remotely manipulate the activities of targeted neurons through light illumination. It combines the technique of genetics and optics to precisely control the well-defined events in biological systems, even in the freely moving animals [6]. As shown in Figure 1, compared to the conventional electrical stimulation, which needs to implant electrodes directly into brains, optogenetics provides a minimally invasive way to deliver the signal to the neurons [5, 7]. Due to the genetic expression limited in specified neural cells, a key advantage of optogenetics is the high selectivity, as opposed to a random set of neurons in electrical stimulation [5, 8]. In addition, because there is a physical limit to the number of micro-electrodes that can be inserted into the brain tissue at one time, the recording of the neural signal in electrical stimulation is limited to a small number of cells.

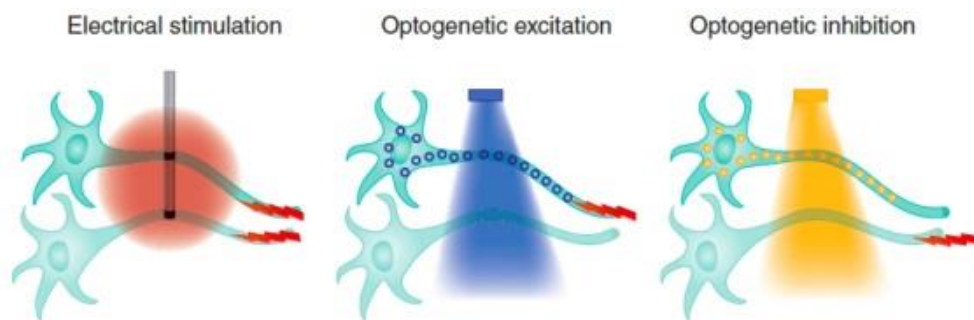


Figure 1 Principle of electrical stimulation and optogenetics [5].

In optogenetics, simultaneous monitoring and stimulation are realized through genetically targeted expression of light sensitive proteins. As shown in Figure 2, the light-sensitive protein is first transfected into living animals by injecting the virus that includes such kind of protein. It can be genetically expressed in targeted neural cells driven by the promoters. These proteins act as rectifying ion channels which can be activated by the light signal with certain wavelength. As a consequence, the stimulated neurons are fired on and thus the movement controlled by those neurons can be achieved [9]. Based on the genetic expression in specified cell types, although the light is incident across a large field, only targeted neurons can be excited.

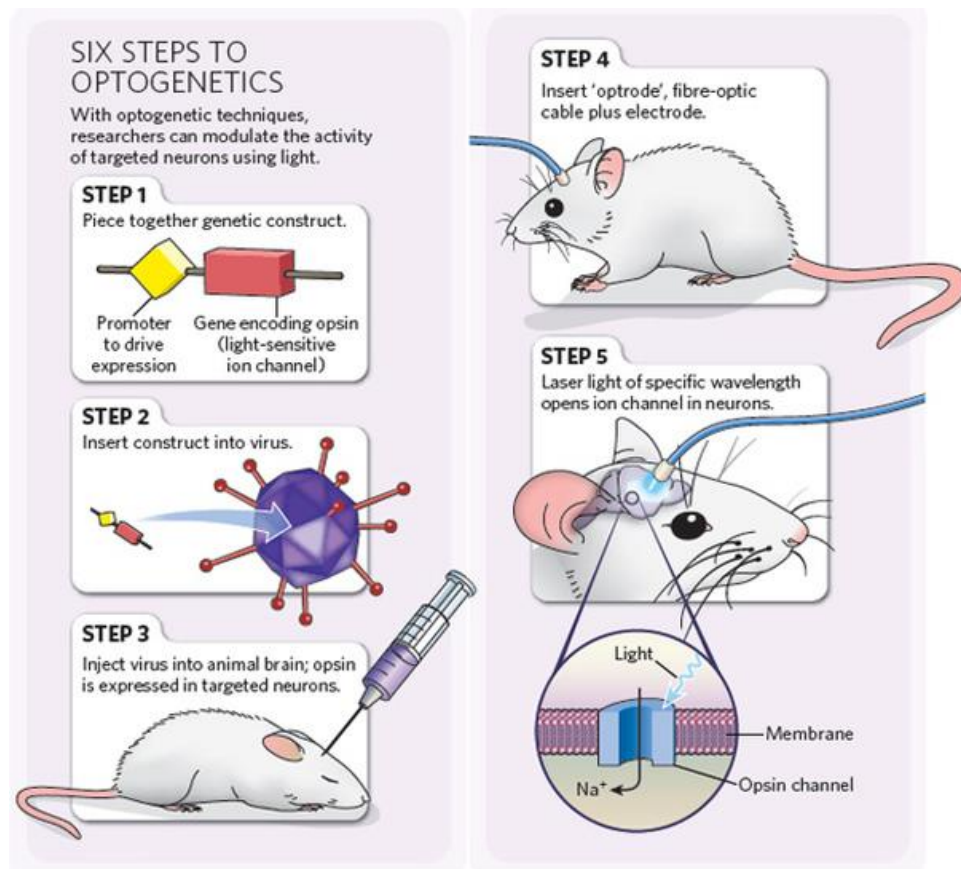


Figure 2 The realization of optogenetics [9].

The current studies on optogenetics popularly use channelrhodopsin-2 (ChR2), a cation

channel highly sensitive to visible light [1-3, 6-9]. In ChR2-expressing neurons, action potentials can be evoked with an excitation power of approximately 1 mW/mm^2 at the maximal absorption wavelength of 470 nm. Thus, illumination with blue light can provide effective excitation, resulting in a permeation of sodium and potassium ions. The high sensitivity of ChR2 has been critical for its successful utilization, especially for *in vivo* studies.

Besides the prospect of basic investigation on structure and function of neuron networks, optogenetics also offers new hopes for patients suffering from vision impairment or neurological disorders based on the potential capability of modulating the activity of brain circuits.

1.1.2 Light sources for optogenetics

The light source used for photo-excitation is a key part of the setup for research on optogenetics. Well-defined spectral, temporal and spatial control is very important as well as homogenous and constant output. Photo-excitation of the neural cells is most commonly accomplished by illuminating the target with a fluorescence lamp or a laser beam with an optic fiber [6, 10, 11]. Although these methods can provide strong illumination and decent positioning of the spot, their size and operation condition is an obstacle for integration on a chip through micro-fabrication.

The employment of light emitting diodes (LEDs) offers an alternate option for optogenetic applications. They are cheaper, smaller, more reliable and easier to control. It can also be incorporated into implants, allowing untethered light delivery in freely moving animals [12]. Especially, arrays of μ -LEDs have been developed which are separately addressable and thus enable multisite stimulation [13-16]. Such spatiotemporal control over large numbers of neurons benefits both basic study of neuron network dynamics and clinical applications such as retinal

prosthesis.

However, a major drawback of LED is its intrinsically low out-coupling efficiency due to light emission with a large beam angle around 90° to 120° , rather than in a coherent beam. Therefore, the amount of light from an LED that eventually reaches the target neurons has been significantly weakened. In addition, since the neural tissue is structurally comprised of several layers of neurons corresponding to different functions, stimulation on targeted layers of neurons is always desired to enable investigation on specified functions [17].

Based on the challenges discussed above, an optical component which can couple with LED and collimate the LED light is demanded. Our group has developed a 3-D multi-waveguide probe array which is able to effectively deliver the light independently from each μ -LED to simultaneously target multiple spots in the brain [16, 18], as shown in Figure 3. However, this waveguide is invasive and could lead to damage to living tissues due to the unavoidable contact.

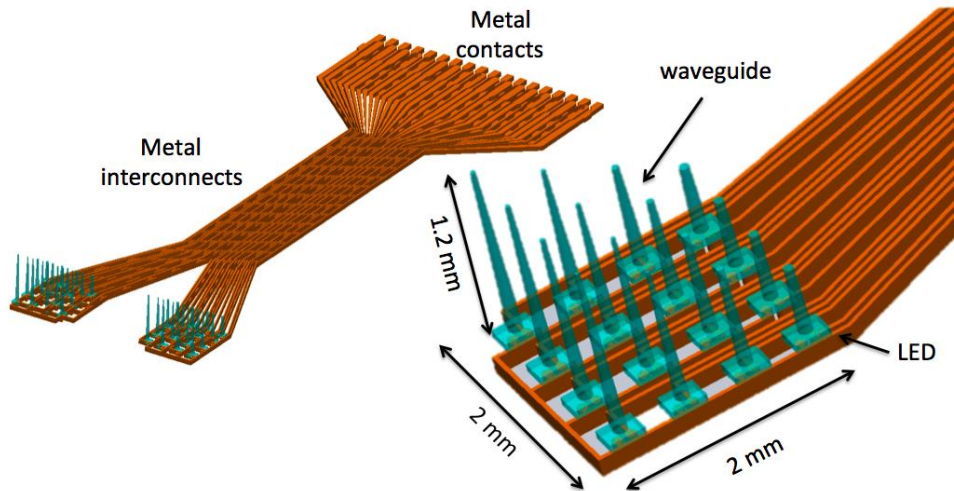


Figure 3 Conceptual diagram of the 3-D multi-waveguide probe array [16].

On the other hand, the large-scale optical lenses coupled with LEDs have already been widely commercialized, with a great majority of them made by molding. However, when the size

scales down to tens or hundreds of micrometer, the quality of molding greatly lowers due to the resolution problem. Little study has been carried out on the fabrication of μ -lens coupled with μ -LED for applications in optogenetics [19, 20]. Appropriate methods for μ -lens fabrication, with the help of microtechnology and the property that is dominant in the micro-scale, need to be explored.

1.2 Objective

In this thesis, a μ -lens array coupled with μ -LEDs is proposed, in order to improve the light out-coupling efficiency. The objective is to fabricate the μ -lens array with specifications suitable for the μ -LED used in our lab. A rapid, low-cost and easily controlled method is pursued. Taking the application into consideration, a fabrication process that is available at low temperature and on a flexible substrate is preferred. With the aid of such μ -lens array, the LED light can be effectively collimated, resulting in an increased light out-coupling efficiency. Multi-depth stimulation at multiple sites within the brain will be further investigated in the following study.

To achieve that goal, efforts have been directed toward exploring the suitable techniques for μ -lens fabrication. A number of techniques, including soft lithography, surface tension modification, thermal reflow, and self-organized dewetting have been studied experimentally and theoretically, which will be discussed in the following chapters.

1.3 Thesis Outline

In chapter 2, lens fabrication by soft lithography will be discussed including the aspects of design, fabrication, simulation and measurement. Surface tension modification on polymeric substrates through plasma treatment will be presented in Chapter 3. Chapter 4 covers the

preparation of μ -lens array by photoresist thermal reflow technique, and Chapter 5 describes the theory, simulation and experiments on the room-temperature self-organized dewetting process on polymer thin films. At the end, in chapter 6 the thesis will be summarized with an outlook of future work and the contribution will be provided.

CHAPTER 2 Lens Fabrication through Soft Lithography

2.1 Background

In the macroscopic scale, an optimized secondary optical lens is of great importance while designing LED lighting fitting [21, 22]. Although LEDs overwhelm classic bulbs in the aspect of directionality, the LED beam angle (around 90° to 120°) is still too wide if used in LED lighting fixture without secondary optics reducing the angle to an acceptable value. In fact, this drawback intrinsically exists, regardless of the scale of the LED. Based on the application, choosing a lens requires awareness of several considerations. However, there are a number of classic design schemes that the commercialized LED lenses always adopt, which can effectively aid to collimate the light rays emitted from LED and improve the out-coupling efficiency.

As shown in Figure 4, a cone-shaped reflecting sidewall is often included in the LED lens design. Effective reflection enables the collection of the incident light with large emitting angles. Meanwhile, a dome-shaped central lens is always employed in the middle to collimate the light rays emitted from LED with small emitting angles. The parameter is designed on the basis of dimensions of luminaire body, lens material, and irradiation characteristics.



Figure 4 Commercialized macro-scale LED lenses, which are often comprised of a central spherical lens and a cone-shaped reflecting sidewall [23].

2.2 Lens Design

2.2.1 Property of LED

The LED employed in this experiment is the model of LB Q39E manufactured by OSRAM Opto Semiconductors. As shown in Figure 5, such device includes a very flat colorless package and has a dimension of $1.6 \times 0.8 \times 0.35 \text{ mm}^3$ (length \times width \times height). A blue light with a wavelength of 470 nm is emitted when applying a voltage larger than 2.7 V. The irradiation characteristic is illustrated in Figure 6. As can be seen, the light escaped from a LED source distributes an angularly lambertian pattern, other than a uniform spherical distribution such as from a point source. Due to the rectangular shape of the LED, the output also varies on different cross-sections perpendicular to the surface of the source.



Figure 5 The LED used in the experiment. It is packaged with a colorless diffused resin.

2.2.2 Optical path design

Inspired by the structure employed on the commercialized macro-scale LED lenses, a compound optic combining a reflecting sidewall and a central lens has been designed to collimate the LED light, as shown in Figure 7. The cavity inside the lens is just suitable for

assembling the LED. The irradiation with small emitting angles can pass through the spherical central lens with the refraction and approach the normal direction, while the light rays with large emitting angles are bounced off the sidewall and gathered through reflection, and therefore the light out-coupling efficiency can be improved.

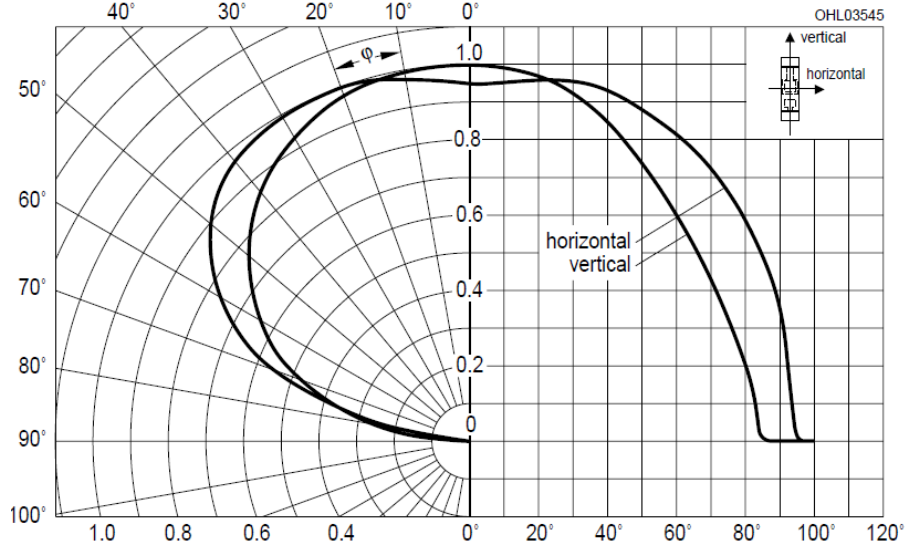


Figure 6 Irradiation characteristic of the LED used in the experiment.

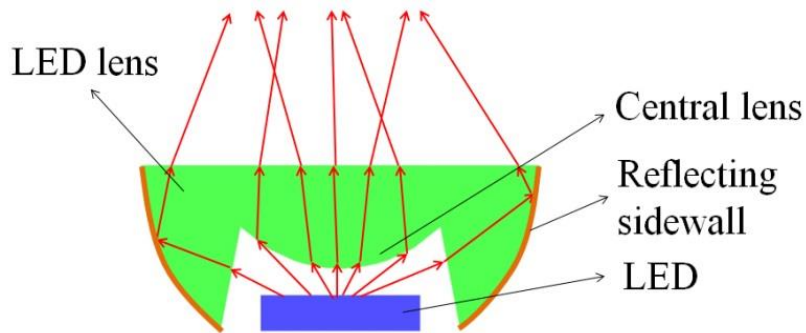


Figure 7 The designed LED lens, which is comprised of a central lens and a reflecting sidewall, in order to collimate the LED light and improve the out-coupling efficiency.

2.2.3 Simulation

Taking the size minimization into consideration, the radius of top surface of the lens, the radius of the base and the height is limited to 2 mm, 1.2 mm and 2 mm, respectively. The radius of the central lens is 1.0 mm. With this dimension, there is sufficient space in the cavity for the LED and soldering. By using the Tracepro software, the influence of the lens on the path of light rays escaped from the surface of LED has been simulated. Considering the variation of distribution on the different cross-sections is slight, as shown in Figure 6 (vertical and horizontal distribution), it is assumed that LED irradiation has a rotational symmetry in this simulation.

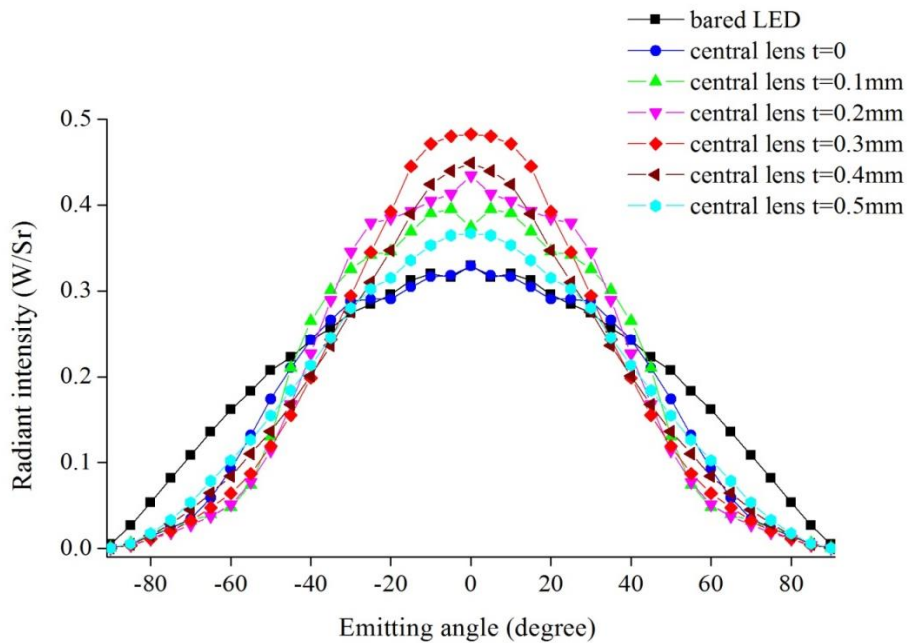


Figure 8 The radiant intensity as a function of light emitting angle of LED, with various curvature of central lens, with different thickness t .

The curvature of the central lens (in terms of the height t) has been optimized by comparing the Candela plots. Figure 8 shows the radiant intensity as a function of light emitting angle of LED, with various curvature of central lens. It can be seen that when the height of the central

lens is 0.3 mm, in which case the radius of curvature is 1.8 mm, the lens shows the best effect on converging the LED light. Such parameter will be employed in the following fabrication. The irradiance map for incident flux on the surface located 5 mm away from the LED is illustrated in Figure 9, which proves the ability of collimation of the lens.

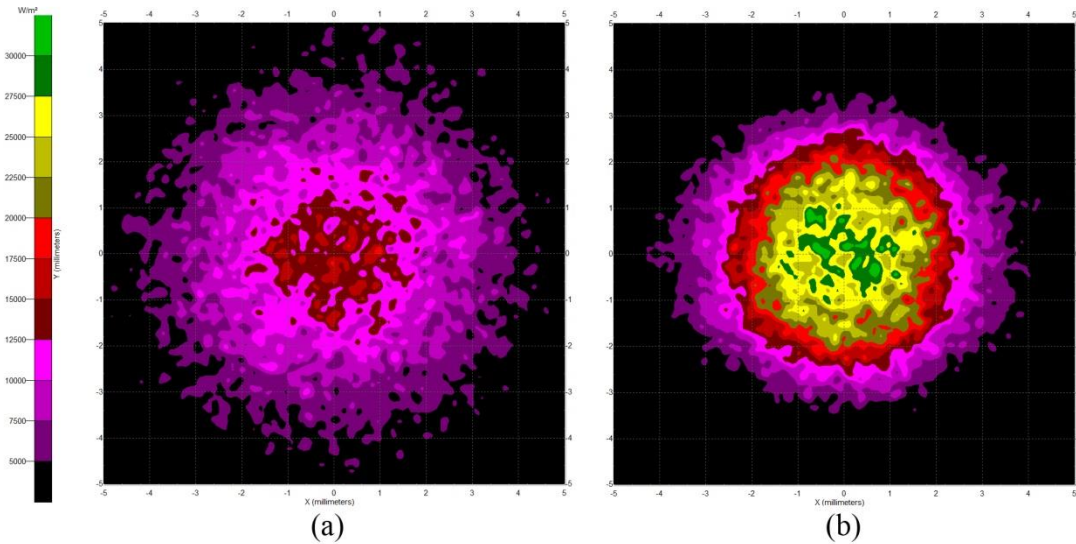


Figure 9 Irradiance map of incident flux on the surface located at 5 mm away from the LED (a) without the lens and (b) with the optimized lens.

2.3 Lens Fabrication

2.3.1 Material

As one of the most commonly used stamp resin in the procedure of soft lithography, polydimethylsiloxane (PDMS) has been chosen as the material for the molding. It is optically clear, inert and non-toxic. Because PDMS can cure very quickly (always less than 1 day without heating), it is particularly suitable for the rapid stamping which enables the transfer of patterns of even a few nanometers in size [24-26].

SU-8 was employed as the material for the lens. It is available in a wide range of viscosity and thickness based on the different percentage of solvent. It has excellent imaging characteristics and is capable of producing high aspect ratio (>20) structures [27-29]. Through the curing by UV light, SU-8 can cross-link and become very hard and stable. It has a refractive index of ~ 1.60 , which was used in the simulation.

2.3.2 Fabrication process

The lens has been fabricated in the following steps, schematically shown in Figure 10.

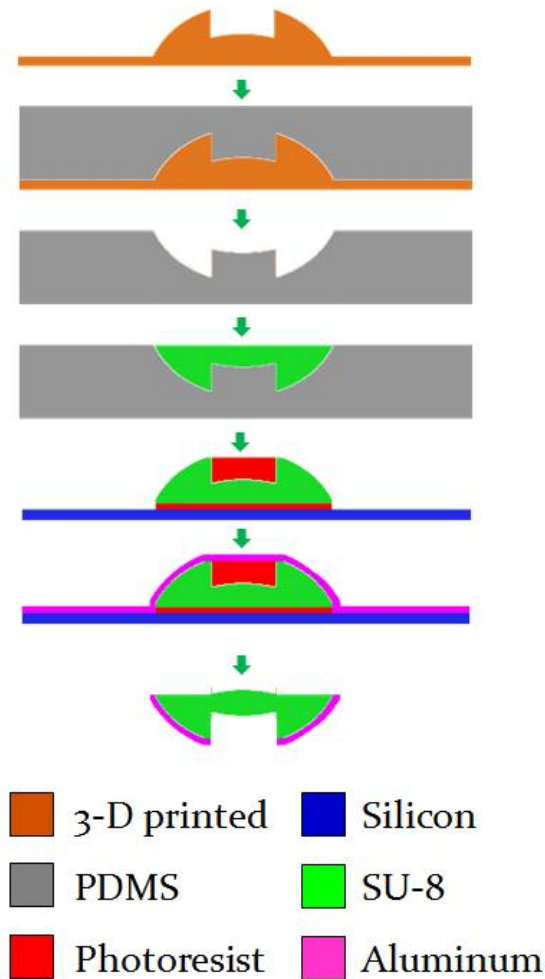


Figure 10 Process flow for lens fabrication.

a) Due to the complexity of the design, 3-D printing was chosen to produce the mold master. Such mold master had the same shape as the lens which would be generated. During the printing, the machine cut the material line by line according to the program. The trace of the tip could be clearly seen on the surface of the mold master and resulted in a quite low resolution, which was not expected.

b) The PDMS base and curing agent were weighed at a ratio of 10:1 and fully mixed through stirring. After that, it was placed into the vacuum oven for degasing until no bubbles appear. PDMS was then carefully poured over the mold master in the petri dish. This step needs to be quite slow in order to minimize introduction of bubbles. The petri dish was placed on the hot plate which was set at 65 °C. PDMS was cured after 1 hour and then peeled carefully off the mold master.

c) SU-8 2075 was filled into the holes on the PDMS master by using the pipette. UV was used to cure the polymer for 90 s. After hard baking at 95 °C in the oven for 10 minutes, it became hard and could be peeled off by tweezers. Until then the basic lens had been fabricated which successfully followed the optimized design through 3-D printing and double reciprocal molding.

d) SU-8 lenses were placed on a level silicon substrate after dipping in photoresist S1813 gently. The photoresist is sticky and can help prevent lenses from falling off the substrate during the metal deposition process. S1813 was also filled into the cavities by pipette.

e) Aluminum deposition was performed to obtain a cover layer of metal. Lift-off method was used to remove the metal above the cavity. After that, the aluminum only resided on the sidewall surrounding the lens, as shown in Figure 11(a).

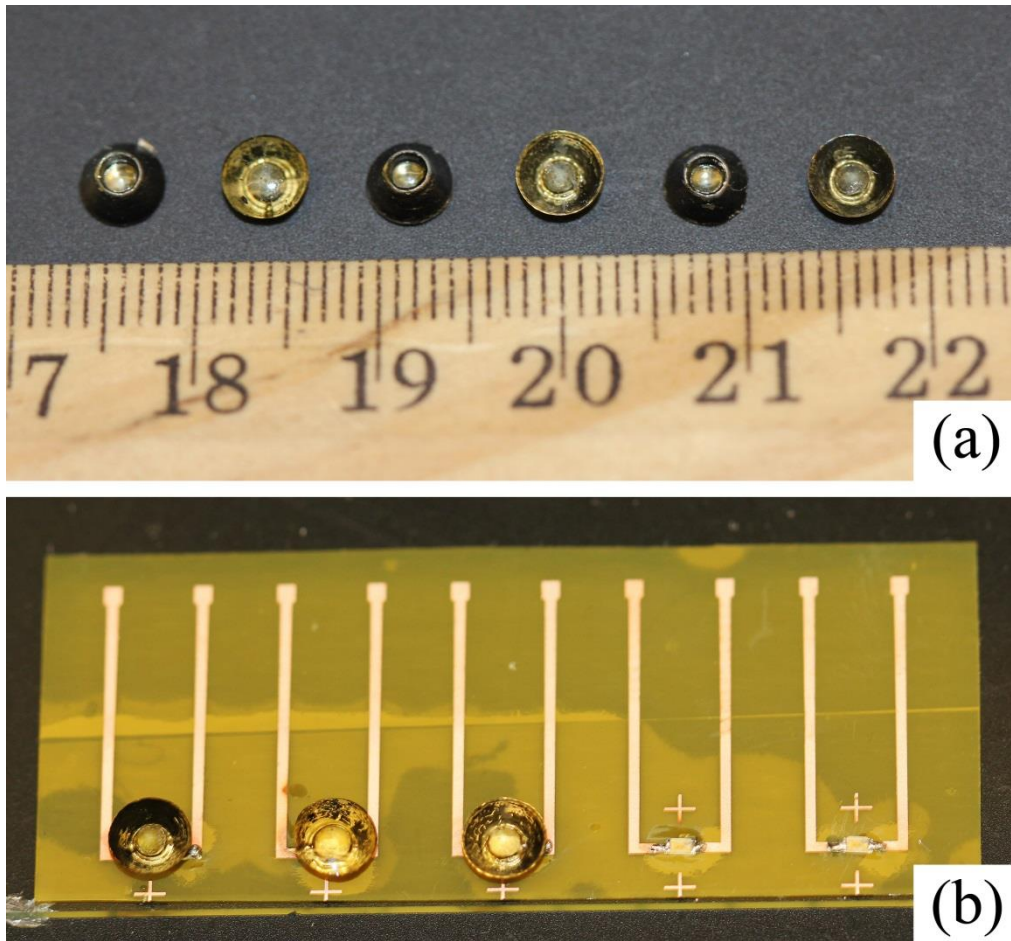


Figure 11 (a) Lenses fabricated by soft lithography; (b) LEDs and Lenses assembled on the polyimide substrate patterned with circuit.

2.3.3 Device assembly

The circuit was prepared by photolithography on the polyimide substrate. A group of LEDs were soldered on their spots by using a low-temperature solder. Then the lenses were positioned on the top of LEDs. The assembled device is shown in Figure 11(b).

2.4 Measurement

The device was vertically placed into the medium of gelatin which was prepared to mimic

the property of natural tissue. A voltage of 2.7 V was applied to light the LEDs simultaneously. The blue light with a wavelength of 470nm was emitted, as shown in Figure 12. The picture was post-processed based on the extraction of blue color in RGB color-space. For each pixel, an integer number in the range 0 to 255 indicates the level of the strength of blue color.

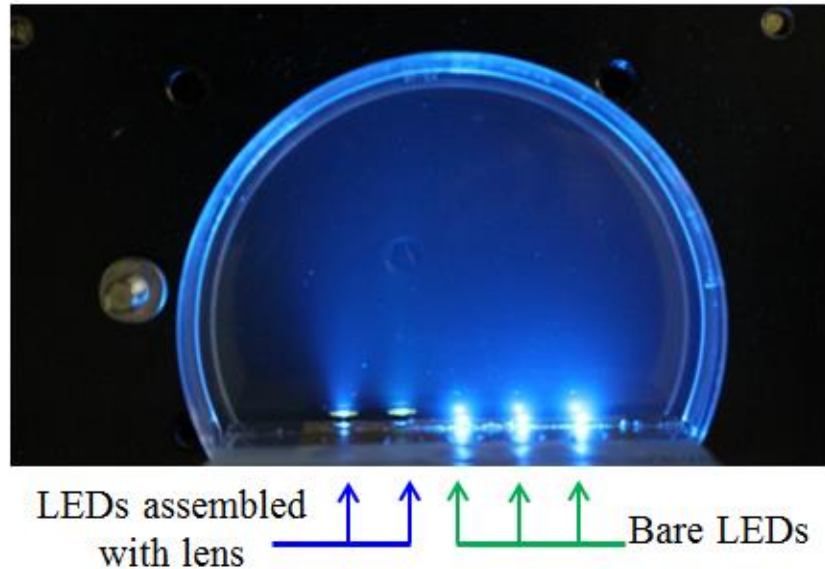


Figure 12 Measurement of light intensity emitted from LEDs with and without coupled lenses. The distribution of light rays clearly shows the converging effect.

Figure 13 shows the distribution of blue light along the normal direction of the device. At the distance longer than 20 cm, the lens-coupled LED exhibits a higher level of the strength of the blue color than bare LED, which can be attributed to the collimating effect of the lens. However, saturation was observed at a short distance for the light emitted from bare LED. It is most likely an artifact as a result of light reflection at the interface, which can be evidenced by Figure 12, in which two symmetric bright spots appear for bare LEDs.

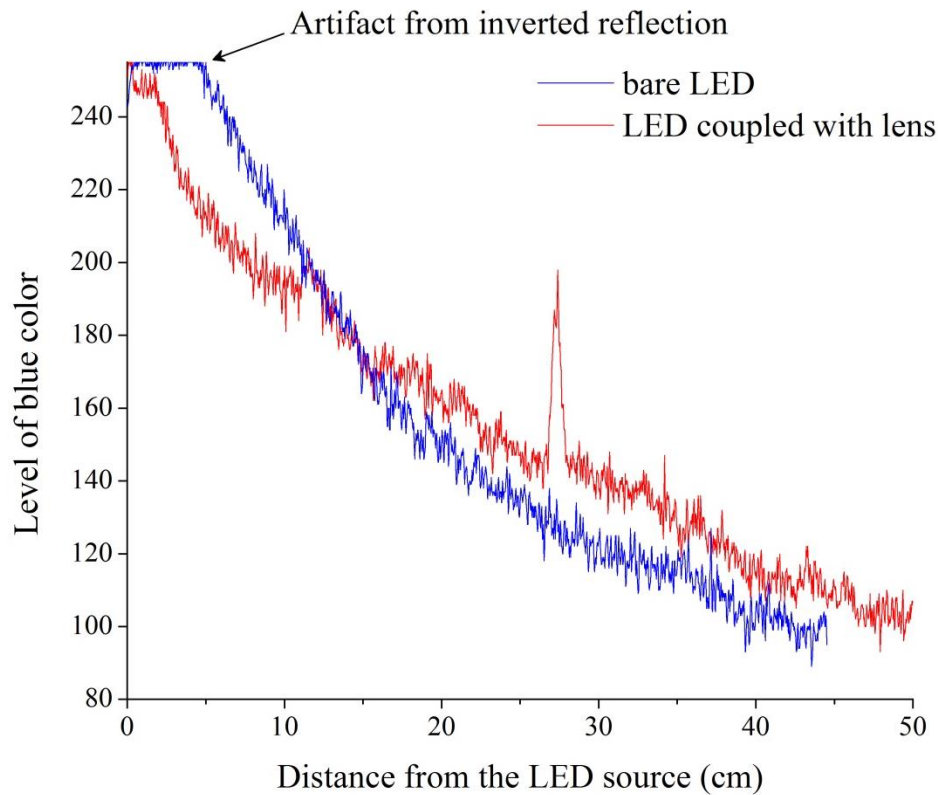


Figure 13 Blue light distribution along the normal direction of the device.

2.5 Summary

Inspired by the design of large-scale commercialized LED lenses, a miniaturized lens was designed in order to improve the light out-coupling efficiency with a dimension fit for the specified LED being used in our lab. Such lens features a reflecting sidewall and a central spherical lens. The parameter was optimized by the simulation result using Tracepro. 3-D printing and soft lithography were employed in the fabrication. The measurement result shows that the lens is able to collimate the light emitted from LED. However, this technique has a major drawback in the aspect of low resolution due to the process of 3-D printing. It has a strong impact to the performance of the device in the small scale. In addition, the whole process is hand-made and somewhat complicated, which is not suitable for batch production.

CHAPTER 3 Surface Tension Modification by Plasma Treatment

3.1 Background

Surface tension is one of the most important attributes of materials. It strongly influences the morphology how a liquid presents on a substrate. Because the droplets are always formed to be nearly spherical caps, contact angle (CA), especially water contact angle (WCA), is often used to characterize the surface tension. Such droplet also offers the possibility of serving as the lens directly. For a given system of solid, liquid, and vapor at a given temperature and pressure, the equilibrium contact angle is unique. Therefore, an effective method which can modify the surface tension is required in order to tune the contact angle of the liquid as needed, leading to various lens curvatures.

Many efforts have been devoted to the development of super hydrophobic surfaces, which have WCAs higher than 150° . Materials with low surface energies, such as polytetrafluoroethylene (PTFE) [30], are often utilized as the outermost layer to increase hydrophobicity. Such coatings, however, greatly limit the possibility of successive processing and/or patterning of substrates. Hence, controlling and tailoring surface wettability directly on original materials is desired for satisfying diverse applications. Two well-established models proposed by Wenzel [31] and Cassie [32] demonstrate a strong correlation between micro- and nano-scale surface morphology and a material's wetting behavior. Inspired by this concept, a variety of engineered surfaces have been reported, utilizing well-defined structures—such as nanotube arrays [33, 34], micropillar patterns [35] and the dual-scale micro- and nano-textured surfaces [36-38]—to achieve super hydrophobicity. However, most of these surfaces require multi-step processes and thus are complicated and expensive. One well-developed surface processing technique is plasma

treatment, which can modify only the most external molecular layers of the material without affecting bulk properties. This process is versatile and can be easily applied on devices with various surface topologies. Many types of plasmas have been found to be effective in altering the surface wettability [39-42]. Nevertheless, in most of the experiments exploring super hydrophobicity, plasma treatment (if employed) is only partially involved as one step of multi-step processes [37, 38]. Plasma treatment alone, despite its convenience and time-efficiency, has not been proven effective for super hydrophobic modification.

3.2 Experiment

A plasma surface modification approach has been proposed to modify the surface tension without altering material bulk properties, which combines an oxygen (O_2) plasma pre-treatment with a sulfur hexafluoride (SF_6) plasma treatment. For ease of exposition, we call this method the “consecutive- O_2 - SF_6 ” (COS) treatment in the following sections. Compared to previously reported methods of achieving super hydrophobic surfaces, our COS treatment eliminates the need for designing complex micro- and/or nano-structures; it is simple and compatible with conventional microfabrication technology and can be applied to both flat and curved surfaces.

3.2.1 Material

As one of the most commonly used polymeric coating materials in biomedical micro- and nano-devices [43-47], Parylene-C has a superb combination of biocompatibility, flexibility, mechanical strength and optical transparency. A unique vapor deposition process is used for the preparation of Parylene-C coatings with pinhole-free conformity and uniform thickness. Parylene-C also provides an excellent dielectric insulation and a consistent barrier against

moisture and chemicals for underlying components. To date, a large number of biomedical devices, such as retinal prostheses [43] and neural probes [46], have employed Parylene-C as the packaging material. Despite the significant development of Parylene packaging techniques, little attention has been paid to the surface modification of Parylene-C [38, 48, 49]. Recently, Lu *et al.* reported a super hydrophobic Parylene-C surface with high and low adhesion by creating hierarchical dual-scale micro/nanostructures [38]. However, the fabrication of such dual-scale structures requires complex processes such as photolithography and DRIE etching, which is very time-consuming and not suitable for treatment on curved surfaces.

3.2.2 Process

Two-inch silicon wafers were chosen as the substrates and cleaned with hydrofluoric acid and deionized water prior to Parylene deposition. 5 μ m-thick Parylene-C films were prepared through vacuum chemical vapor deposition (CVD) using a PDS 2010 Labcoter[®] 2 (Specialty Coating Systems). During this process, the raw material dimer dichloro-di(p-xylylene) is first vaporized at 150 °C under vacuum and then pyrolyzed at 690 °C to generate the monomeric form chloro-p-xylylene. The monomer subsequently condenses at room temperature onto the wafer substrates in the deposition chamber to form conformal Parylene-C thin films. The thickness of Parylene-C films was determined by the amount of initial loading of dimer and verified by a profilometer.

The COS treatment was performed in a reactive ion etching (RIE) system (LAM 9400, LAM Research Corporation) using O₂ plasma followed by SF₆ plasma. During the experiments, the chamber was evacuated to a base pressure of 10 mTorr before introducing the process gas with a constant flow rate of 100 sccm. A fixed radio-frequency (RF) power of 100 W was used

during all plasma processes. The O₂ plasma pre-treatment of Parylene-C films was carried out first. The treatment duration varied from 20 s to 10 min for several groups of samples. After that, SF₆ plasma was applied to the samples for 1 min. Separately, in the experimental study of switchability, a Parylene-C sample was pre-treated with O₂ plasma for 10 min, and then SF₆ and O₂ plasma treatments were alternately conducted for 1 min each on the same surface.

3.2.3 Measurement

Both the static and dynamic WCAs were measured with a contact angle analysis system (VCA 2000, AST Products, Inc.) immediately after plasma treatments to characterize the surface wettability of modified Parylene-C films. A 2 μL droplet of deionized water was dispensed onto the Parylene-C surface with a vertical syringe. The side view of the droplet was recorded by the equipped digital image acquisition system and subsequently analyzed to determine the contact angle.

The surface morphology was characterized by an AFM (Dimension 3100, Bruker Nano). A scanning area of 3 μm by 3 μm was randomly selected on the substrates. The root-mean-square (RMS) surface roughness and quantitative three-dimensional (3-D) images were obtained. The surface chemistry on Parylene-C films was examined with an XPS (Phi 5600 ESCA system, Perkin Elmer) using a monochromatic magnesium K α X-ray source.

3.3 Results

3.3.1 Static WCA measurements

Prior to any treatments, the Parylene-C surface exhibited a WCA of 89.0±0.5°. Complete wetting (WCA ~ 0°) was observed after O₂ plasma pre-treatment of 40 s or longer. In this case,

the water droplet spread on the surface instantly on contact, indicating a super hydrophilic surface had been produced. This phenomenon is mainly attributed to the introduction of oxygen-related polar functional groups onto the surface during the plasma treatment [50], which is consistent with previously reported results for surface hydrophilic modification of polymers by O₂ plasma [51-53].

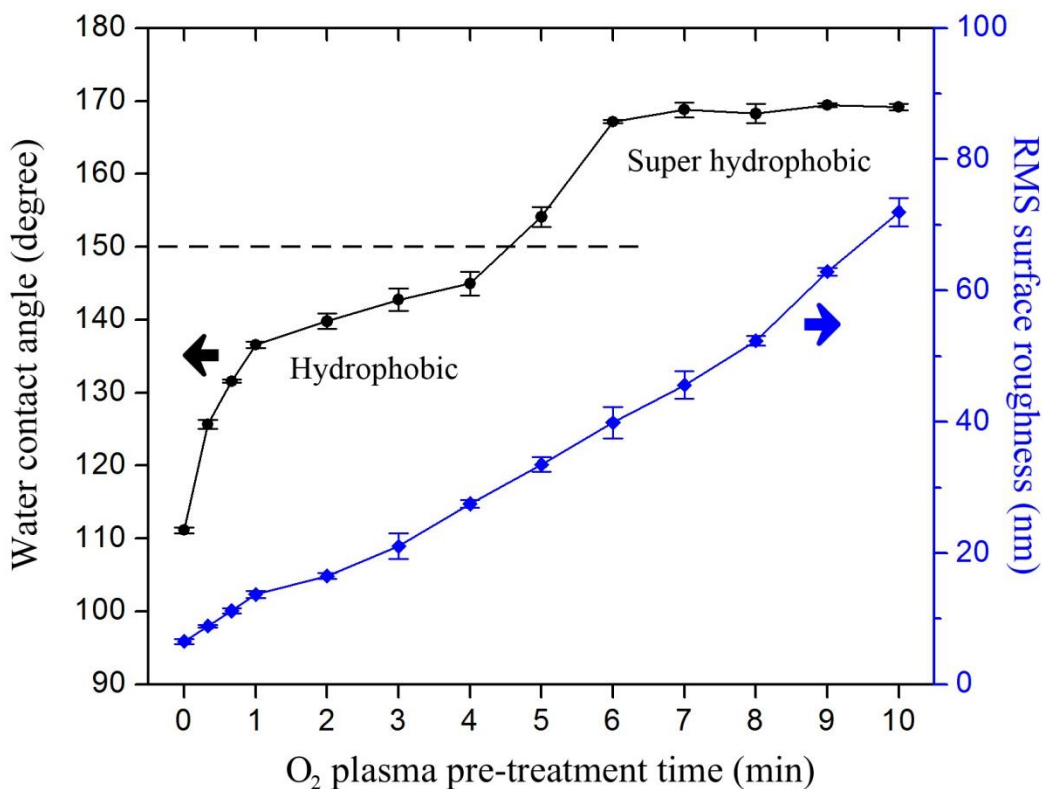


Figure 14 WCAs and RMS surface roughness on O₂ and SF₆ plasma-treated Parylene-C thin films as a function of the O₂ plasma pre-treatment time.

Subsequently, 1 min SF₆ plasma treatment was performed on the O₂ plasma pre-treated Parylene-C surfaces. The measured static WCAs are plotted as a function of O₂ plasma pre-treatment time in Figure 14. It can be seen that this brief process led to a complete inversion of the wetting behavior on Parylene-C from hydrophilicity to hydrophobicity. The WCA became

progressively higher with increased O₂ plasma pre-treatment time. It exceeded 150° when 5 min O₂ plasma pre-treatment was performed, indicating that the Parylene-C surface had turned to super hydrophobic. After 7 minutes, the WCA saturated around 169°. The highest WCA measured in our work was 169.4±0.3°.

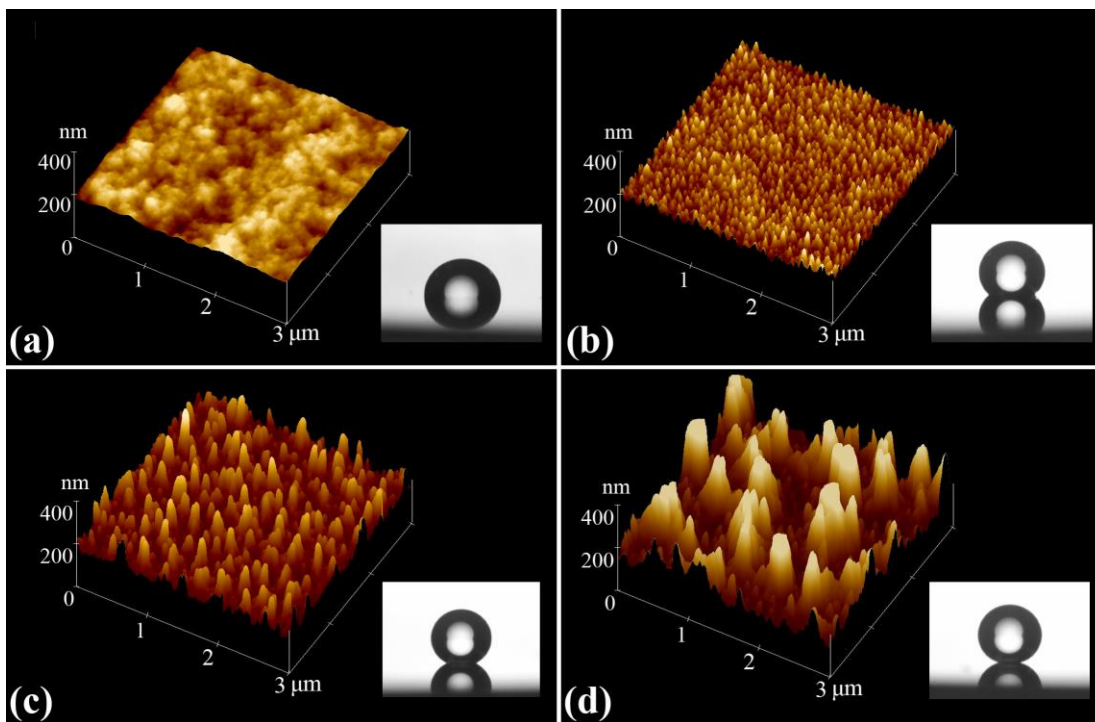


Figure 15 The representative 3-D images of Parylene-C surfaces and corresponding WCA images, with (a) no treatment, and plasma-treated with (b) 1 min O₂ + 1 min SF₆, (c) 5 min O₂ + 1 min SF₆, and (d) 10 min O₂ + 1 min SF₆.

3.3.2 Surface roughness

The effects of plasma treatment on the surface morphology were examined by AFM. The change of RMS roughness is plotted in Figure 14. After polymer deposition, the fresh Parylene-C displayed a cotton-like surface with an RMS roughness of 5.772±0.376 nm. Upon exposure to the plasma, columnar structures appeared on the surface. As shown in Figure 15, the height of

these structures increased with longer O₂ plasma pre-treatment time, resulting in a significant increase in the roughness. The RMS roughness increases at approximately 6.54 nm per minute of O₂ plasma pre-treatment time. On the other hand, the SF₆ plasma treatment increased the surface roughness very slightly, at about 0.76 nm per minute. This great difference can be attributed to the higher chemical reactivity of O₂ plasma with polymers, a property that makes it a popular choice for polymer etching [54, 55]. It can be concluded that the O₂ plasma treatment played a primary role in roughening the Parylene-C surface in this COS process.

3.3.3 Surface chemistry

The representative XPS survey spectra and corresponding fitted high-resolution carbon 1s (C1s) spectra of Parylene-C surfaces are presented in Figure 16. Compared to the untreated Parylene-C film (Figure 16(a)), a significant increase in the oxygen (and fluorine) atomic concentration was observed on the O₂ (and SF₆) plasma-treated surface (Figure 16(b) and (c)), which reveals the formation of new functional groups formed through the plasma-surface interaction. In the high-resolution C1s spectra, the peaks were labeled with corresponding chemical bonds where the carbon atoms were positioned. As can be seen, a number of new peaks arose after the plasma treatment. For the surface treated with only O₂ plasma, the deconvolution of C1s spectrum indicates the presence of two new peaks at 287.8 eV and 289.3 eV, which can be attributed to the carbon atoms in the free carbonyl group (C=O) and carbonate group (O₂C=O), respectively. The forming of these functional groups increased the polarity of the Parylene-C surface and thus raised the surface free energy, resulting in the improved wettability [50].

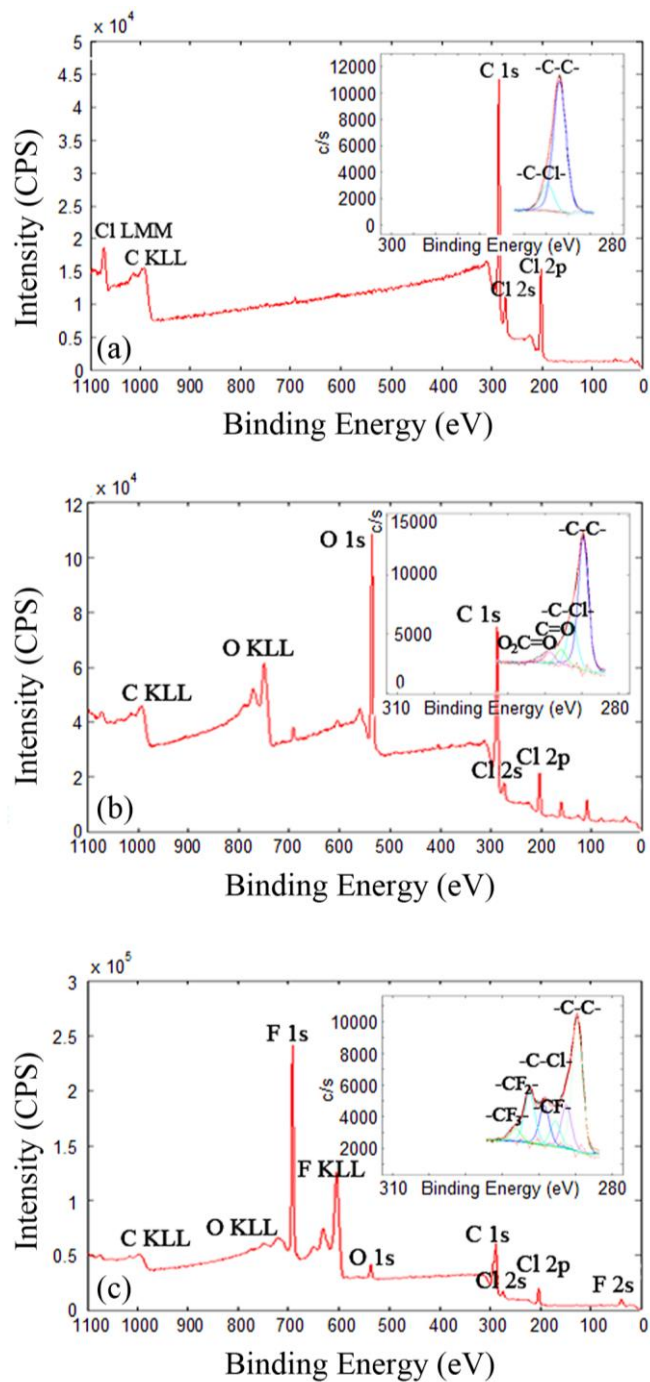


Figure 16 The representative XPS survey spectra and corresponding fitted high-resolution C1s spectra (inlets) of Parylene-C surfaces with (a) no treatment, and plasma-treated with (b) 10 min O₂ and (c) 10 min O₂ + 1 min SF₆. The peaks are labeled with corresponding elements in survey spectra and carbon-related functional groups in high-resolution C1s spectra.

Similarly, new peaks representing the carbon atoms in the groups of -CF-, -F-C-Cl-, -CF₂- and -CF₃- showed up in the spectrum of the Parylene-C film that had been treated with both O₂ and SF₆ plasmas, corresponding to the peaks at 287.8eV, 289.3eV, 291.3eV and 293.2eV, respectively. Due to the chemical inertness, the fluorinated groups help lower the surface energy and thus enhance the hydrophobicity [56, 57]. While SF₆ was selected as the main fluorinated gas source in this work, other fluorinated gases such as C₄F₈ are expected to react with the polymer surface in a similar way, as reported elsewhere [39]. It is noteworthy that the O₂ plasma treatment was a critical step prior to SF₆, which not only helped to create a rough surface but also reactivated the inert Parylene-C surface to enable subsequent chemical reaction with fluorine ions.

3.3.4 Switchability

We have proven previously that the COS treatment can effectively modify the surface wettability of Parylene-C films to super hydrophobicity. On that basis we proceeded to study the switchability between super hydrophobicity and super hydrophilicity through alternating one-minute SF₆ and O₂ plasma treatments on a Parylene-C sample pre-treated with O₂ plasma for 10 min. The variation of WCAs with successive treatments is shown in Figure 17. It can be seen that a 1 min post-treatment can successfully switch the surface wetting property between super hydrophilicity and super hydrophobicity. The WCAs did not show any deterioration after five cycles.

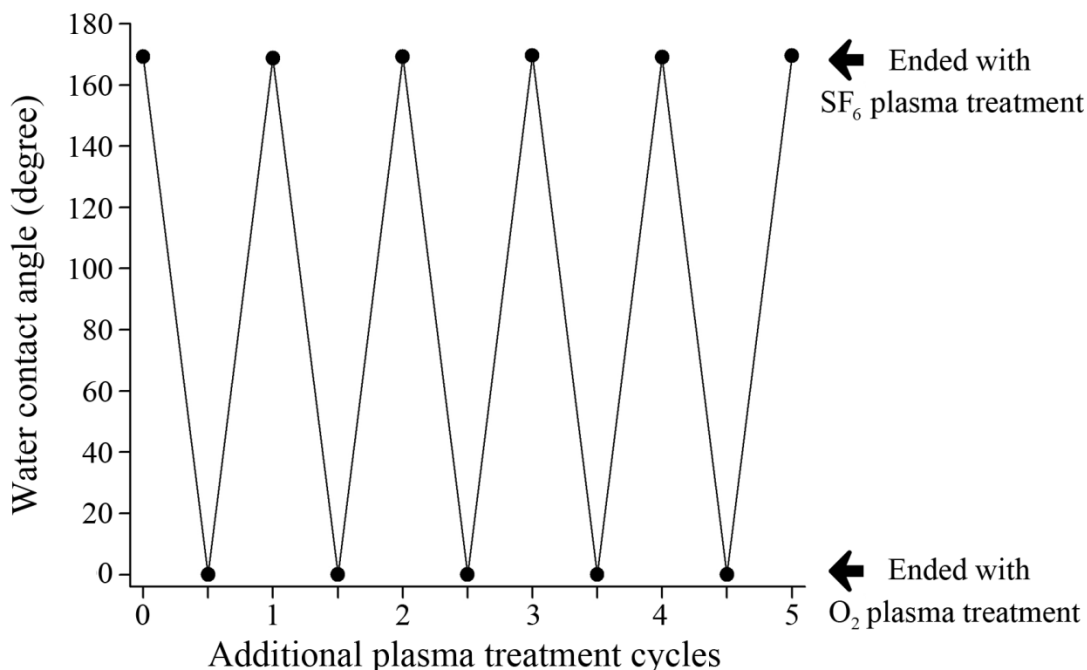


Figure 17 The switchability between super hydrophobicity and super hydrophilicity on Parylene-C thin films. The original point corresponds to the Parylene-C surface plasma-treated by 10 min O₂ + 1 min SF₆. Afterward, O₂ and SF₆ plasma treatments were alternately conducted for 1 min each on the same sample.

3.4 Analysis

As discussed above, the COS treatment is able to modify the surface wetting property of Parylene-C films to super hydrophobicity by enhancing the surface roughness and altering the surface chemistry. The O₂ plasma pre-treatment offers several key functions in this work. It efficiently increases the surface roughness of the Parylene-C, which is essential to achieve super hydrophobicity on a solid surface, as suggested by previous work [31-39]. It also effectively activates the inert polymer surface by forming new oxygen-related chemical bonds, which improves the efficiency of the subsequent reaction with the SF₆ plasma. The O₂ plasma treated

surface exhibited a super hydrophilic property as the result of the increased surface roughness and activation. Following the O₂ plasma pre-treatment, the 1 min SF₆ plasma treatment completely converted the surface wettability to hydrophobic by introducing fluorinated functional groups, without significant change of the surface roughness. In this section, the droplet state on such rough and hydrophobic surfaces has been investigated based on two well-established models, the Wenzel model and the Cassie model. The Wenzel model holds for homogeneous wetting (wetting contact status), where the liquid remains in full contact with the rough surface. The apparent contact angle θ_w can be given quantitatively by the Wenzel equation [31]:

$$\cos\theta_w = r \cos\theta_E, \quad (1)$$

where θ_E is the equilibrium contact angle on a flat, rigid and homogeneous surface, the wettability of which is solely dependent on the chemical composition; r is the roughness factor defined as the ratio of the actual liquid-solid contact area to the projected area on the horizontal plane. The Cassie model holds for heterogeneous wetting (composite contact status) where liquid cannot penetrate the whole surface and air pockets are trapped among the roughness peaks underneath the droplet. In this case, the apparent contact angle θ_C is given by the Cassie equation [32]:

$$\cos\theta_C = fr_w \cos\theta_E + f - 1, \quad (2)$$

where f is the area fraction of the solid-liquid contact on the horizontal projected plane, r_w is the ratio of the actual liquid-solid contact area to the projected area, θ_E is as described in the Wenzel equation. Of these two states, the droplet usually prefers the one with the lower surface energy (in most cases, it also corresponds to the lower contact angle), which is determined solely by the surface topology. Due to the difference of contact status, the droplet in the Cassie state shows

less contact angle hysteresis (defined as the difference between the advancing WCA and the receding WCA) than in the Wenzel state and thus rolls off the surface with greater ease.

The WCA hysteresis was studied by measuring the dynamic WCAs on the COS-treated Parylene-C thin films in relation to the surface roughness induced by the O₂ treatment (Figure 18). Based on the determination of the contact angle hysteresis, the surface free energies (SFEs) of the as-treated Parylene-C solid surfaces can be estimated using the following equation [58]:

$$\gamma_s = \gamma_1 (\cos \theta_r - \cos \theta_a) \frac{(1 + \cos \theta_a)^2}{(1 + \cos \theta_r)^2 - (1 + \cos \theta_a)^2}, \quad (3)$$

where γ_s is the free energy of the solid surface, γ_1 is the surface tension of the deionized water (~72.8 mN/m at room temperature), θ_a is the advancing contact angle, and θ_r is the receding contact angle. Figure 19 presents the predictive curve of the SFEs (γ_s), corresponding to various durations of the O₂ plasma treatment on Parylene-C surfaces.

Furthermore, Figure 20 illustrates the relationship between the roughness factor r and the value of minus cosine of the static WCAs ($-\cos\theta$), as well as the WCA hysteresis. Here the roughness factor was obtained directly from AFM analysis software through the integral of surface height distribution over the scanning area. As can be seen, two regions are clearly distinguished by the dashed line on both curves. To the left of the line, $-\cos\theta$ is linearly proportional to the roughness factor r , indicating that the Wenzel equation was followed and the surfaces were in the Wenzel state. The slope represents the value of $-\cos\theta_E$ where θ_E is the static WCA on a theoretical ideally flat ($r = 1$) Parylene-C surface that is chemically the same as the surface treated by O₂ and SF₆ plasmas. This value is ~0.314, indicating that the WCA on the assumed surface (θ_E) is ~108.3 °(shown by the diamond in Figure 20). This approximate linearity, in accordance with Eq. (1), also implies that the surface chemistry is nearly consistent among all hydrophobic samples regardless of how long they had been pre-treated by O₂ plasma prior to SF₆

plasma treatment. Therefore, it can be concluded that the surface roughness, primarily caused by the O₂ plasma treatment, plays a dominant role in the surface wetting property and thus scales the static WCA ($-\cos\theta$) by roughness factor r . In addition, it has been found that the WCA hysteresis rises and remains above 40 degrees, further confirming the Wenzel state of the droplets. This can be explained by the pinning effect on the moderately roughened surface, which makes the surface sticky and thus increases the difference between advancing and receding WCAs.

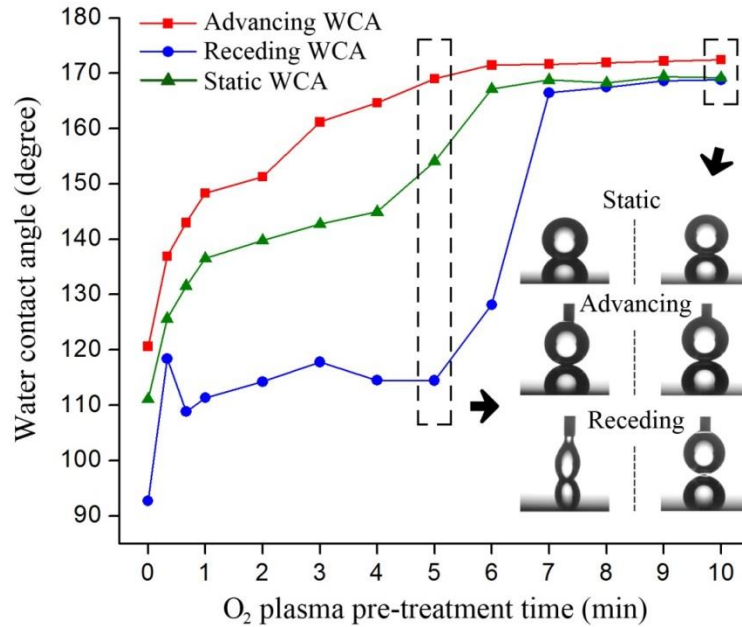


Figure 18 The advancing, receding and static WCAs on COS-treated Parylene-C thin films as a function of the O₂ plasma pre-treatment time. The insets show the representative WCA images on Parylene-C surfaces plasma-treated with 5 min O₂ + 1 min SF₆ (left) and 10 min O₂ + 1 min SF₆ (right), which correspond to the water droplets in the Wenzel state and Cassie state, respectively.

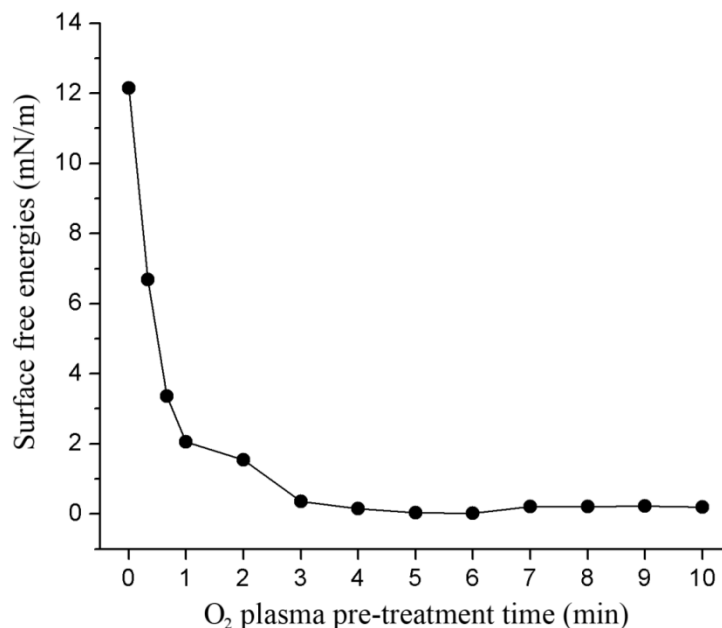


Figure 19 The predictive surface free energies (SFEs, γ_s) on COS-treated Parylene-C thin films as a function of the O₂ plasma pre-treatment time.

As the roughness factor r continued to increase, $-\cos\theta$ gradually saturated in the vicinity of 0.98 and the WCA hysteresis dramatically decreased to only ~ 3 degrees (on the right of the dashed line in Figure 20), implying that the status of droplets has experienced a transition from the Wenzel state to the Cassie state on super hydrophobic Parylene-C surfaces. The critical point of this transition corresponds to a roughness factor of ~ 1.45 and a WCA of $\sim 168^\circ$. When the roughness exceeds this critical point, the droplet cannot wet the entire surface beneath it, mainly due to trapped air in the rough surface. Therefore, the solid-liquid adhesion weakens with a low WCA hysteresis. As a result, the droplet becomes much easier to roll off the surface, carrying away the surface contaminants.

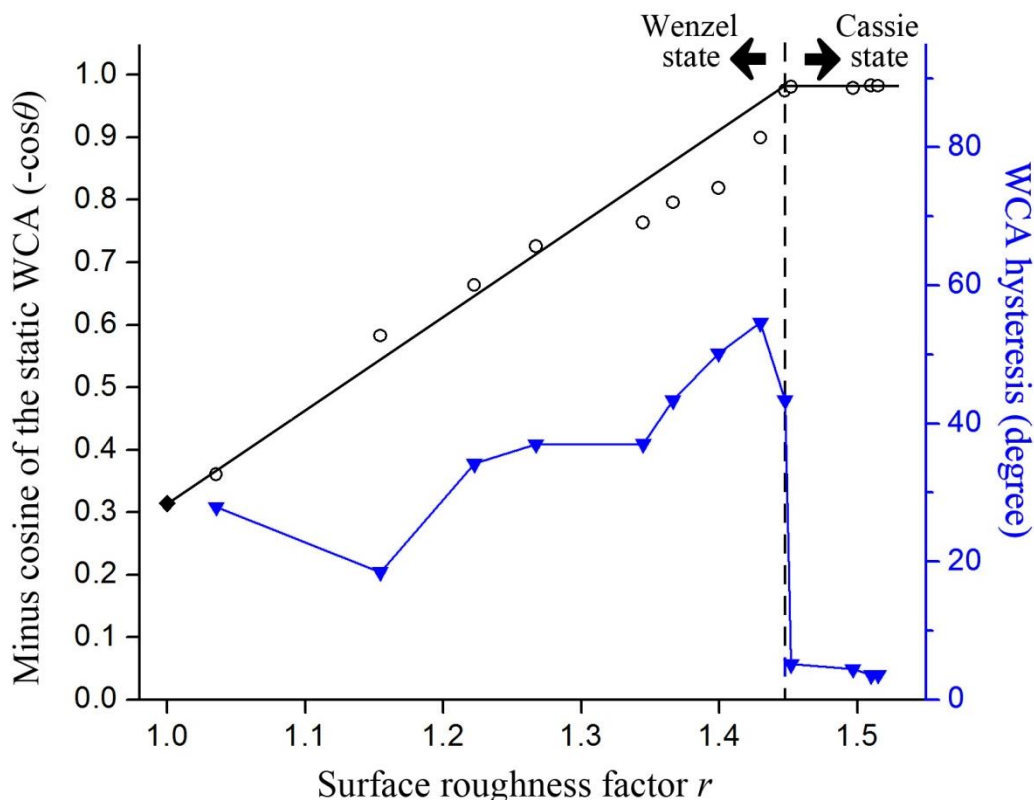


Figure 20 The value of minus cosine of the static WCA and WCA hysteresis on COS-treated Parylene-C surfaces as a function of the surface roughness factor r . The points also correspond to the various pre-treatment time by O_2 plasma from 0 (leftmost), 20 s, 40 s, 1 min, 2 min to 10 min (rightmost). The diamond point represents the extrapolated value on a theoretical ideally flat ($r = 1$) Parylene-C surface, which is chemically the same as the surface treated by O_2 and SF_6 plasmas. Two regions are distinguished by the dashed line on both curves, implying a transition of droplet status from the Wenzel state to the Cassie state.

3.5 Summary

We have demonstrated a simple and time-efficient method in which low-powered O_2 and SF_6 plasma treatments were utilized to realize the surface tension modification. Our combination approach is able to achieve super hydrophobic Parylene-C surfaces without conventionally

patterning micro- or nano-scale structures. Experimental results demonstrated that the physical roughening and chemical modification were the two main factors contributing to the significant variation of WCAs. The COS-treated surfaces displayed a nearly uniform chemical composition. The surface roughening treatment with O₂ plasma has been demonstrated to have a magnification effect on the surface hydrophobicity following the Wenzel equation, until the surface WCA saturates at a high value of ~169°. A transition of droplet status from the Wenzel state to the Cassie state was also observed on the hydrophobic Parylene-C surfaces, characterized by the WCA saturation and the dramatic decrease of WCA hysteresis.

Due to the evaporation, water is not ideal as the lens material unless the device is sealed. Polymer liquids, which do not evaporate but can be cured, have the potential to replace water in lens preparation. They can also show different contact angles on substrates with different surface tension, such as on the plasma-treated Parylene-C. However, it is difficult to accurately dispense polymer liquid with a given volume by simply using the syringe or pipette due to high viscosity. Therefore, a micro-fabrication method that is able to obtain polymer liquids with accurate volume and pattern them into spherical shapes is particularly desired. In Chapter 4 and 5, the techniques of photoresist thermal reflow and self-organized dewetting will be explored to fabricate polymer-based μ -lenses, respectively. The method of modifying surface tension through plasma treatment, discussed in this chapter, will be involved and employed.

CHAPTER 4 Fabrication of Micro-lens Array through Thermal Reflow

4.1 Background

As an important process in micro-optics, thermal reflow is a simple and cost-effective technique by which the photoresist cylinder, created through photolithography, is baked above its glass transition temperature (T_g). This technique, which is based on mass transport, was first described by Popovic *et al.* in 1988 [59]. The molecular chain of the resist can slide past each other with ease when the temperature is above T_g , in which case the polymer is in the rubber-like state with a stronger mobility than in the solid state. During the reflow, surface tension plays a dominant role in transforming the photoresist into the final shape, especially for micro-patterns in which case the gravitational effect is negligible. This method can help obtain high resolution without the loss of process margin. A spherical lens-shaped structure is always gradually formed during the process if circular patterns have been generated, as shown in Figure 21 [60]. The curvature of the lens is largely dependent on the baking temperature and the surface tension of both photoresist and substrate. Positive photoresists which do not crosslink are generally very suitable for the reflow.

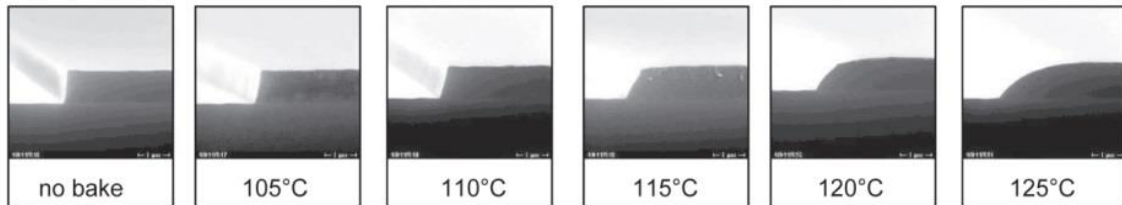


Figure 21 The evolution of the cross-section of photoresist structures during the reflow process, as the baking temperature increases [60].

Fabrication of μ -lenses with diameters ranging from 5 μm up to 1 mm has been reported

with thermal reflow technique [61-64]. Arrays of μ -lenses can also be produced in mass production, as shown in Figure 22 [61], which enable independent function of illumination and imaging. The variation of initial geometry can be incorporated in mask design and spin-coating process.

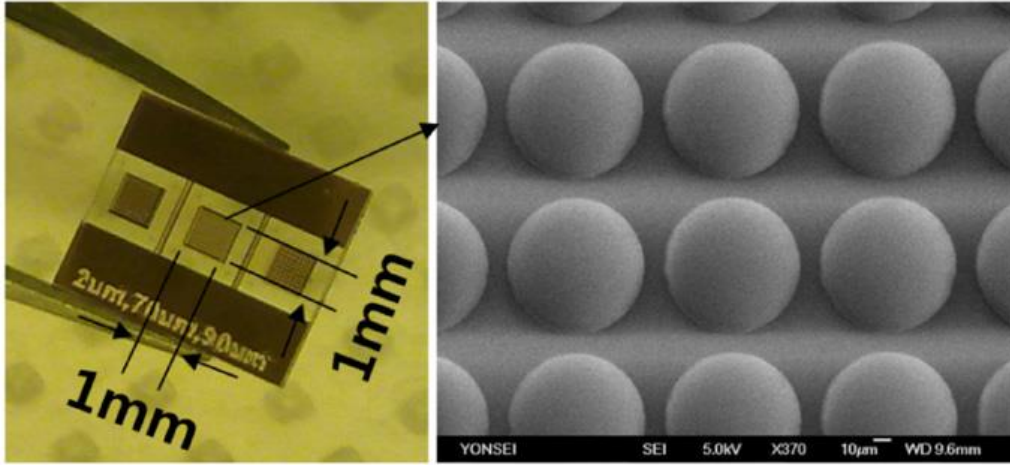


Figure 22 The reported μ -lens array with lens diameter of 80 μm fabricated through thermal reflow [61].

4.2 Experiment

AZ4620 was chosen as the reflow material. Several substrates with different surface tension were used for the thermal reflow process, including silicon, PDMS and Parylene-C. AZ4620 was first spin-coated at 1,000 rpm for 40 sec to obtain a layer of $\sim 17 \mu\text{m}$ thick photoresist on substrates. The thickness can be varied by adjusting the speed of spin-coating. The samples were baked at $100 \text{ }^\circ\text{C}$ for 2 min and then allowed to slowly cool down until room temperature on the hot plate in order to prevent from photoresist cracking. A photomask including circular patterns with different diameters ranging from $200 \mu\text{m}$ to $500 \mu\text{m}$ was used in photolithography. The AZ4620 photoresist was exposed by UV light for 90 sec with a dosage of $1,500 \text{ mJ/cm}^2$. After

developing, the cylinder array was achieved on the substrate. Finally, the samples were transferred into the oven and heated up to 160 °C for 3 days. The photoresist cylinders gradually reflowed and the profile was changed into a spherical lens-shape as a result of the surface tension effect. The process flow is illustrated in Figure 23.

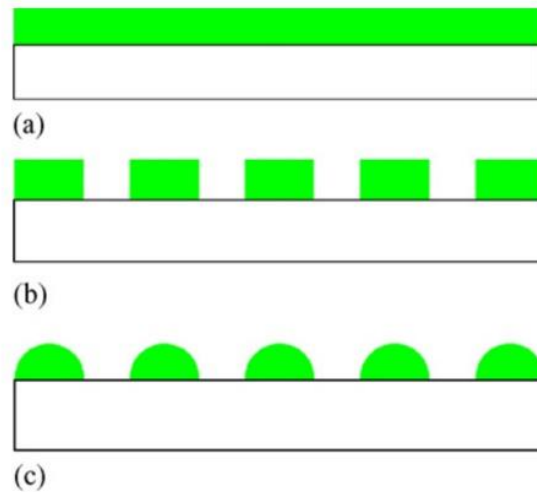


Figure 23 Schematic illustration of the formation of μ -lens array produced by photoresist thermal reflow technique: (a) AZ4620 was spin-coated on the substrate; (b) photoresist cylinders were obtained after photolithography; (c) during the reflow, the profile of patterned photoresist was changed into spherical lens-shape due to the surface tension effect.

4.3 Results and Analysis

4.3.1 Microscopic view

The micro-patterns of AZ4620 photoresist with various diameters were observed under the microscope before and after thermal reflow process, as shown in Figure 24. It can be seen that after the thermal reflow process, the patterns look softer and smoother. The irregular edge disappeared and displaced by a smooth transition.

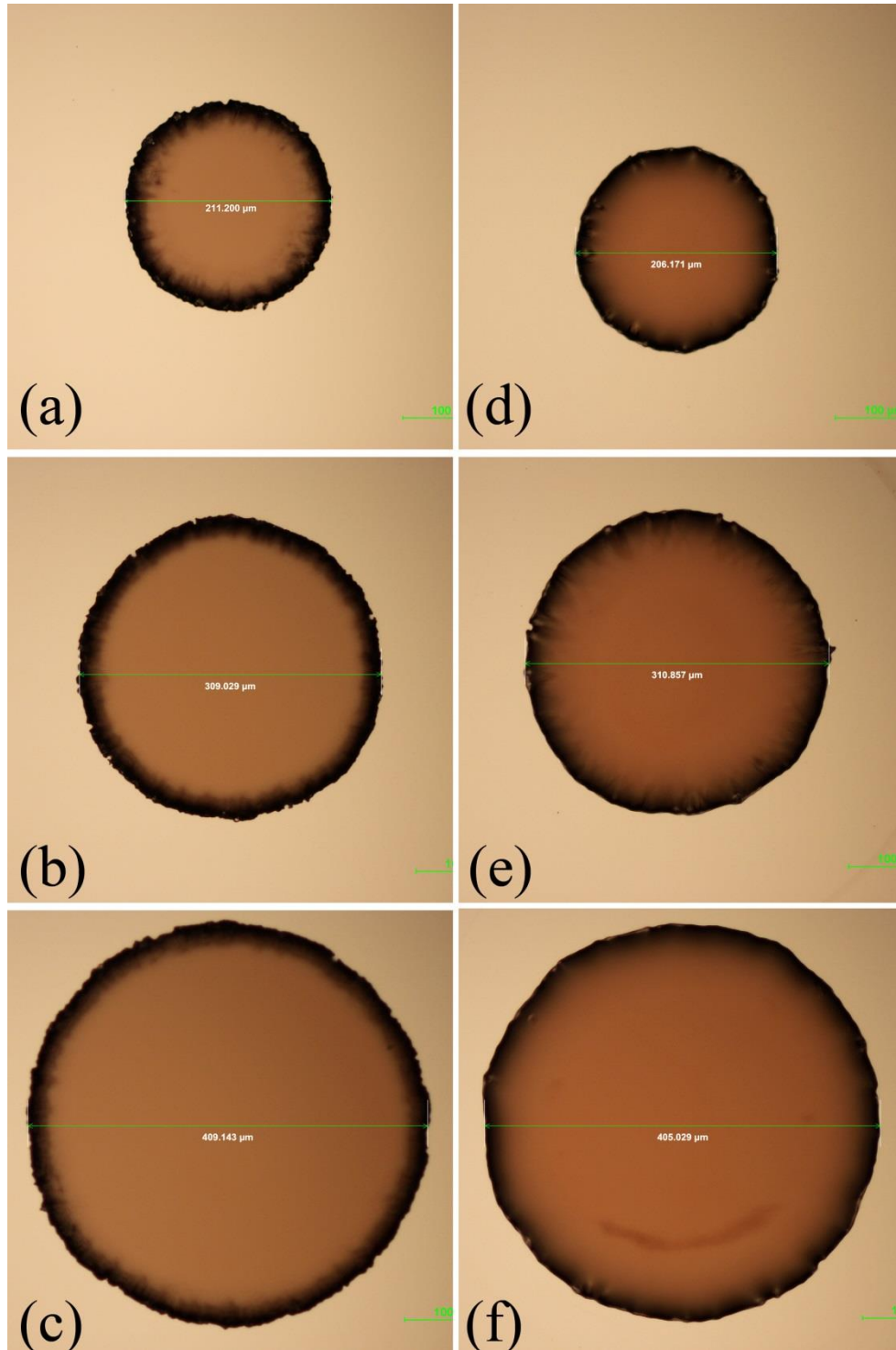


Figure 24 Microscopic view of AZ4620 micro-patterns (a)-(c) before and (d)-(f) after reflow on the silicon substrate. The diameters are (a) (d) 200 μm , (b) (e) 300 μm , and (c) (f) 400 μm , respectively.

4.3.2 Profile

The profile of micro-patterns on silicon substrates was measured by the stylus profilometer, as shown in Figure 25. As can be seen, the lenses were gradually formed during the reflow. For the micro-patterns with initial diameters of 200 μm and 300 μm , spherical lens-shape has been achieved after thermal reflow at 160 $^{\circ}\text{C}$ for 3 days. However, for the micro-patterns with an initial diameter of 400 μm , hollows still existed in the top middle, implying that reflow process had not finished. It can be attributed to the insufficient mobility of the photoresist. Either longer time or higher temperature is required to fully convert the pattern into the spherical lens-shape.

The reflow process has also been carried out on PDMS substrates, which has a lower surface tension than silicon. It is noteworthy that the measurement by profilometer could not be done before the reflow because the stylus could push the patterns off PDMS easily during the scanning, due to a low adhesion between AZ4620 photoresist and PDMS. Figure 26 shows the final profile of μ -lenses after thermal reflow at 160 $^{\circ}\text{C}$ lasting for 3 days. The spherical lens-shape has been obtained for all the samples with initial diameters of 200 μm , 300 μm and 400 μm , without the appearance of hollows on the top middle. It is also worth noting that the photoresist shrank greatly during the reflow in order to form a higher lens on the PDMS, implying that surface tension plays an important role in the reflow process. The curvature can be estimated in terms of contact angle based on the geometry of spherical cap. Figure 27 summarizes the contact angle of μ -lenses made by AZ4620 through thermal reflow process. The photoresist exhibits a contact angle of $\sim 70^{\circ}$ on PDMS substrate, which is much larger than that on silicon substrate.

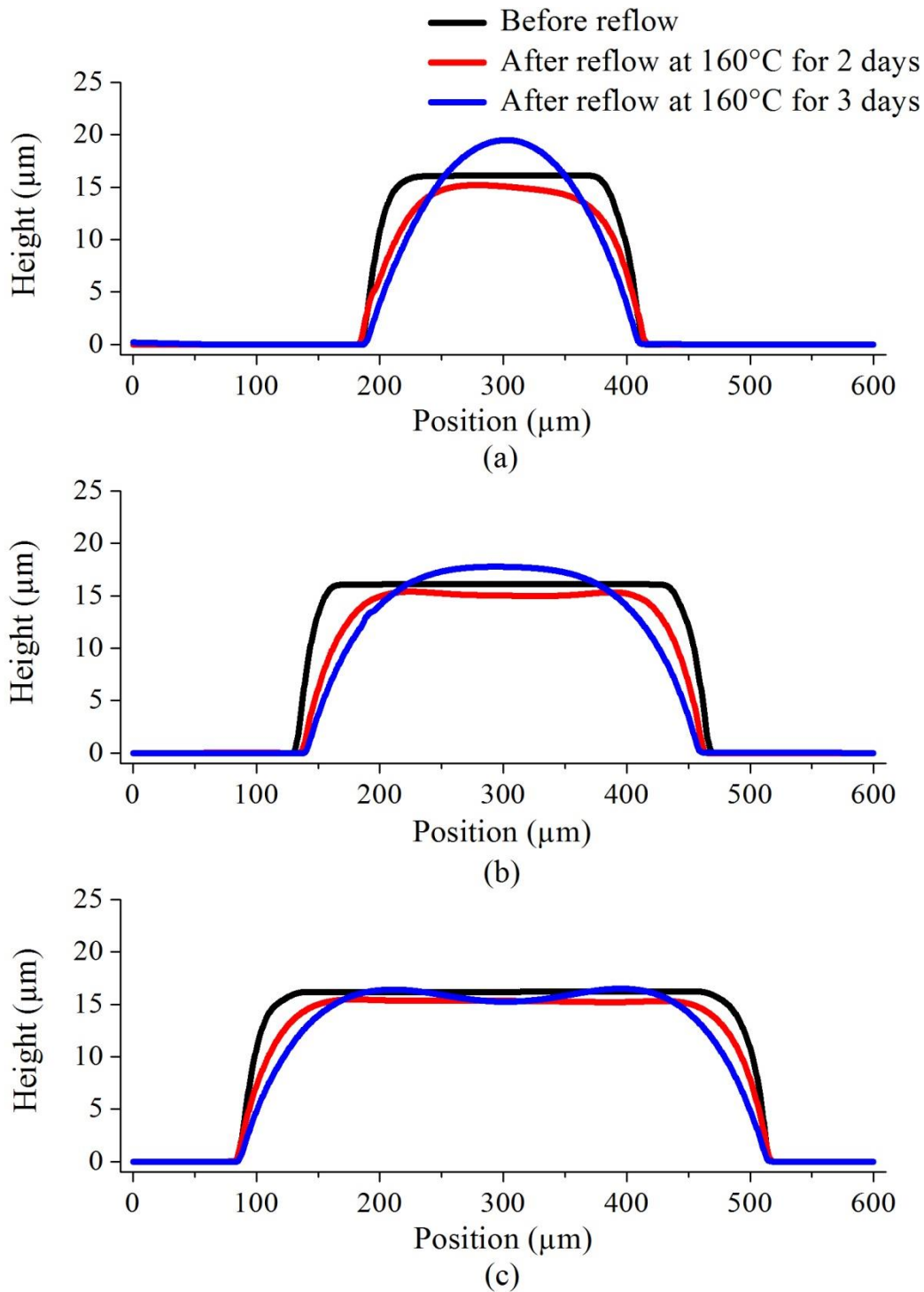


Figure 25 The profile of micro-patterns with various initial diameters of (a) 200 μm , (b) 300 μm and (c) 400 μm on silicon substrates during thermal reflow. (a) and (b) spherical lens-shape was finally achieved; (c) hollows still existed on the top middle.

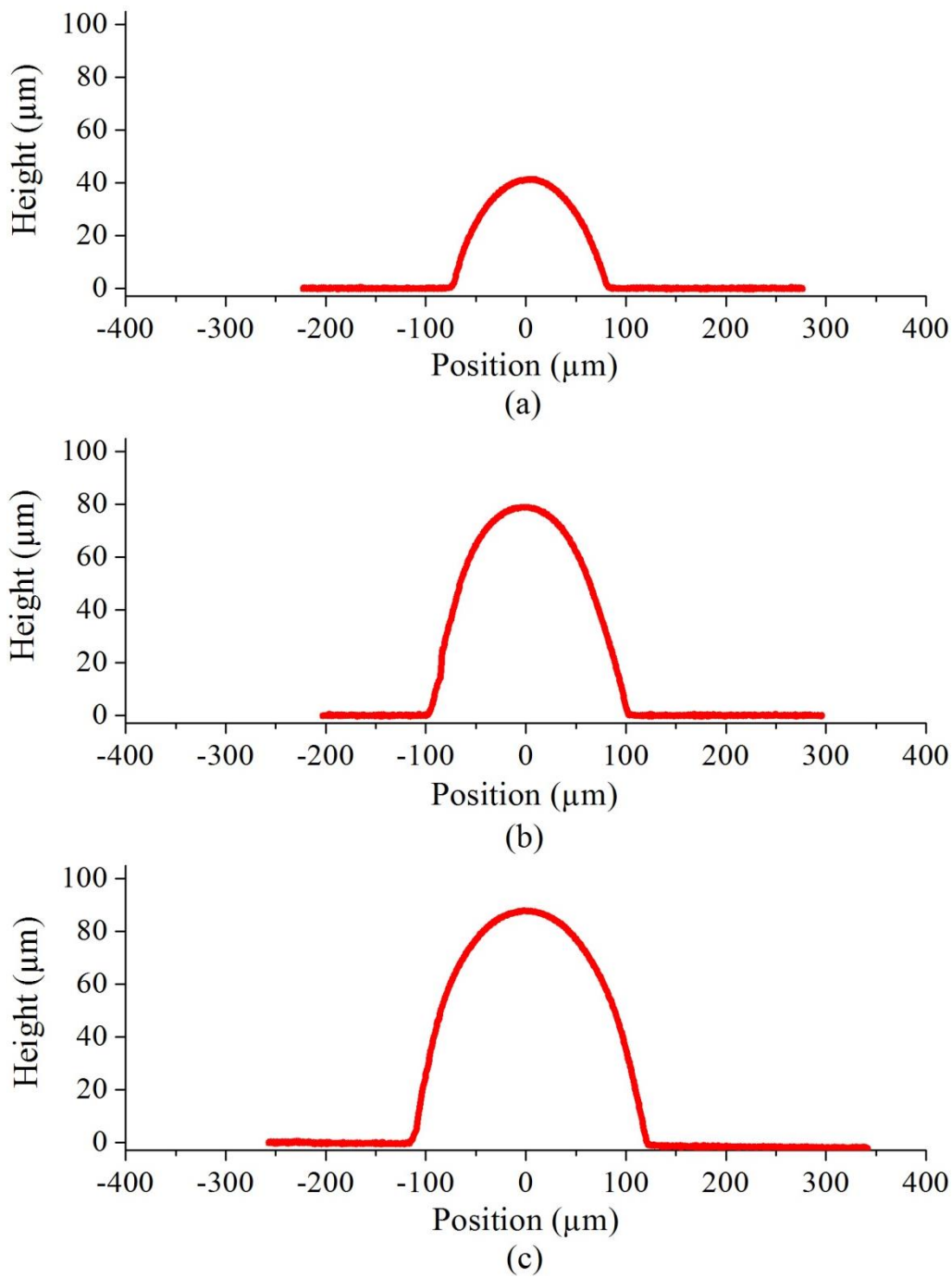


Figure 26 The final profile of μ -lenses with various initial diameters of (a) 200 μm , (b) 300 μm and (c) 400 μm on PDMS substrates after thermal reflow at 160 $^{\circ}\text{C}$ lasting for 3 days.

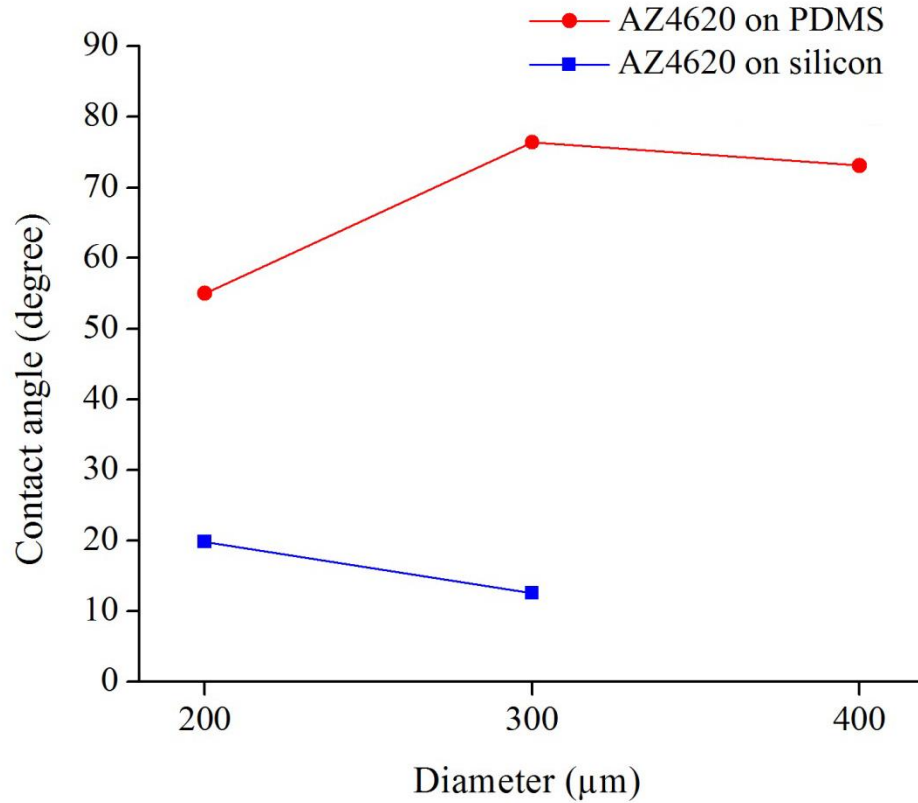


Figure 27 Contact angles of μ -lenses on silicon and PDMS substrates. The lenses were made by AZ4620 through thermal reflow process with 160 °C lasting for 3 days.

4.3.3 SEM images

The morphology of fabricated μ -lens array was observed by scanning electron microscopy (SEM). The SEM images of μ -lenses with an initial diameter of 200 μm on silicon, PDMS and Parylene-C substrates are shown in Figure 28.

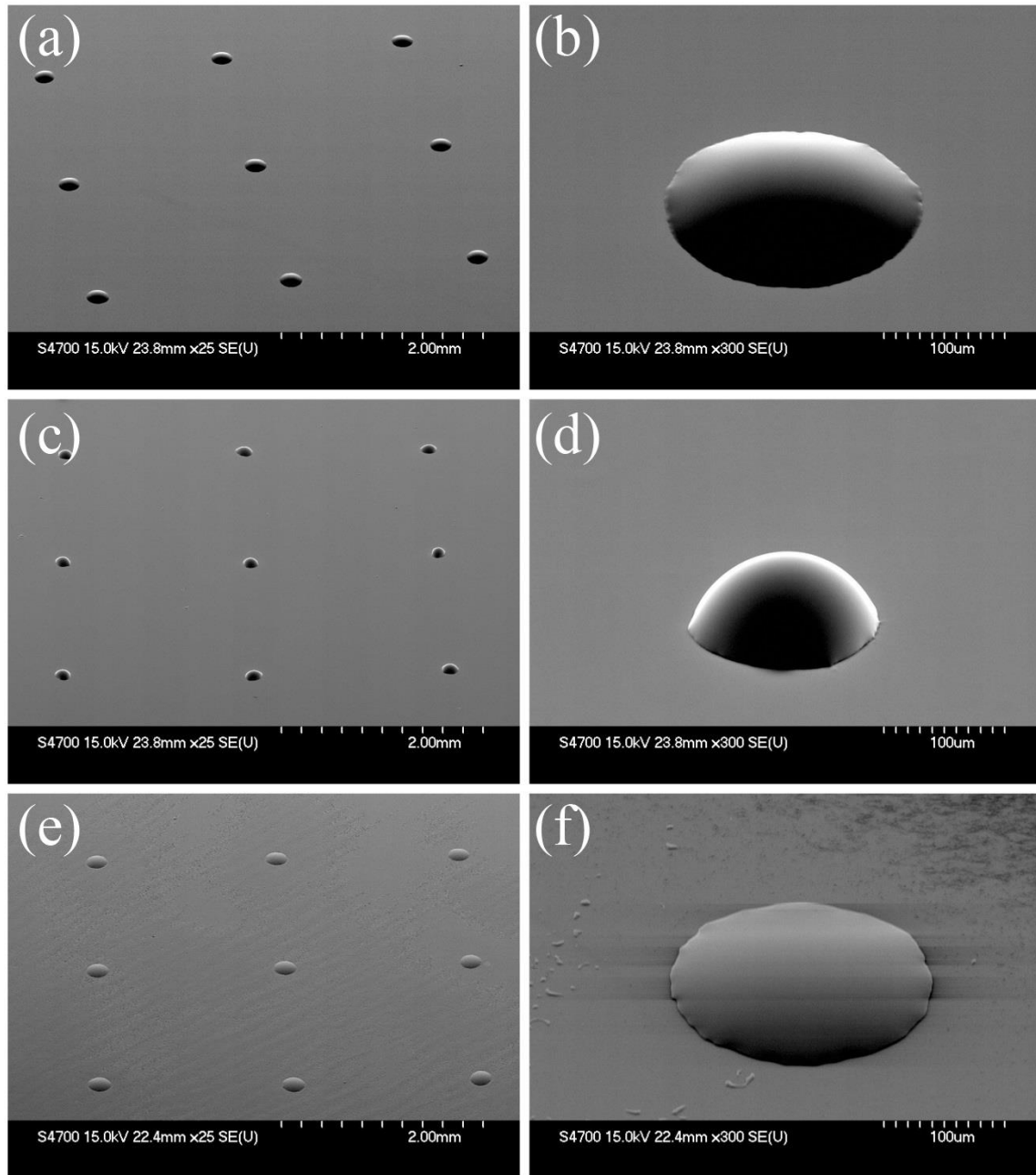


Figure 28 SEM images of fabricated μ -lens array and single μ -lens with an initial diameter of 200 μm on (a) silicon, (b) PDMS, and (c) Parylene-C substrates. Such μ -lens array was made by photoresist AZ4620 and achieved through the thermal reflow technique.

4.4 Summary

The μ -lens array made by photoresist AZ4620 has been achieved through thermal reflow technique. The photoresist was patterned by photolithography and then baked over its glass transition temperature for a couple of days. Surface tension plays an important role in the evolution of the profile of micro-patterns during reflow. A spherical lens-shape can be obtained if the driving force is strong enough for the mass transport. Because thermal reflow process is only suited for positive photoresist and common positive photoresists such as AZ4620 are not transparent, soft lithography needs to be combined to transfer the lens-shape and duplicate it by other transparent materials for optical applications. In addition, another disadvantage of thermal reflow technique is the high temperature, such as 160 °C in the previous experiment, which could likely cause permanent damage to the device.

CHAPTER 5 Fabrication of Micro-lens Array through Dewetting

5.1 Background

It is a common phenomenon that water is reluctant to be everywhere when used to flush some non-hydrophobic surface. It often forms a number of droplets randomly on certain spots. In fact, more generally, a thin liquid coating tends to break up and fails to remain continuous on the surface if the spreading coefficient is negative. This phenomenon is called “reticulation” or “dewetting”. If the surface property is uniform, dewetting may ultimately lead to a set of randomly isolated droplets. If the surface is chemically patterned with various surface tension, during the dewetting the droplets tend to stay on the areas with low contact angles. Therefore, if combined with the technique of surface tension treatment previously introduced, dewetting of polymer liquid films could provide a fast and self-organized route to fabricate μ -lens arrays.

5.2 Experiment

5.2.1 Dewetting of SU-8 on PDMS

If a liquid coating is transparent and curable, it can be directly used as the lens material after the formation of lens-shaped droplets during the dewetting process. Therefore, SU-8 3005 was chosen as the liquid coating material for the dewetting experiment. As illustrated in Figure 29, PDMS surface was first patterned by photolithography. O_2 plasma treatment was carried out and the wettability of exposed PDMS surface turned into hydrophilic. After that, the photoresist was rinsed off and SU-8 was spin-coated on the pre-patterned PDMS surface. Finally, dewetting took place when the substrate was heated up to 105 °C in the oven. The whole dewetting process lasted for 5 min before the completion. Figure 30 shows SEM images of the PDMS surface after

dewetting. As can be seen, the SU-8 μ -lens array was self-organized onto the surface area that had been pre-treated by the O₂ plasma.

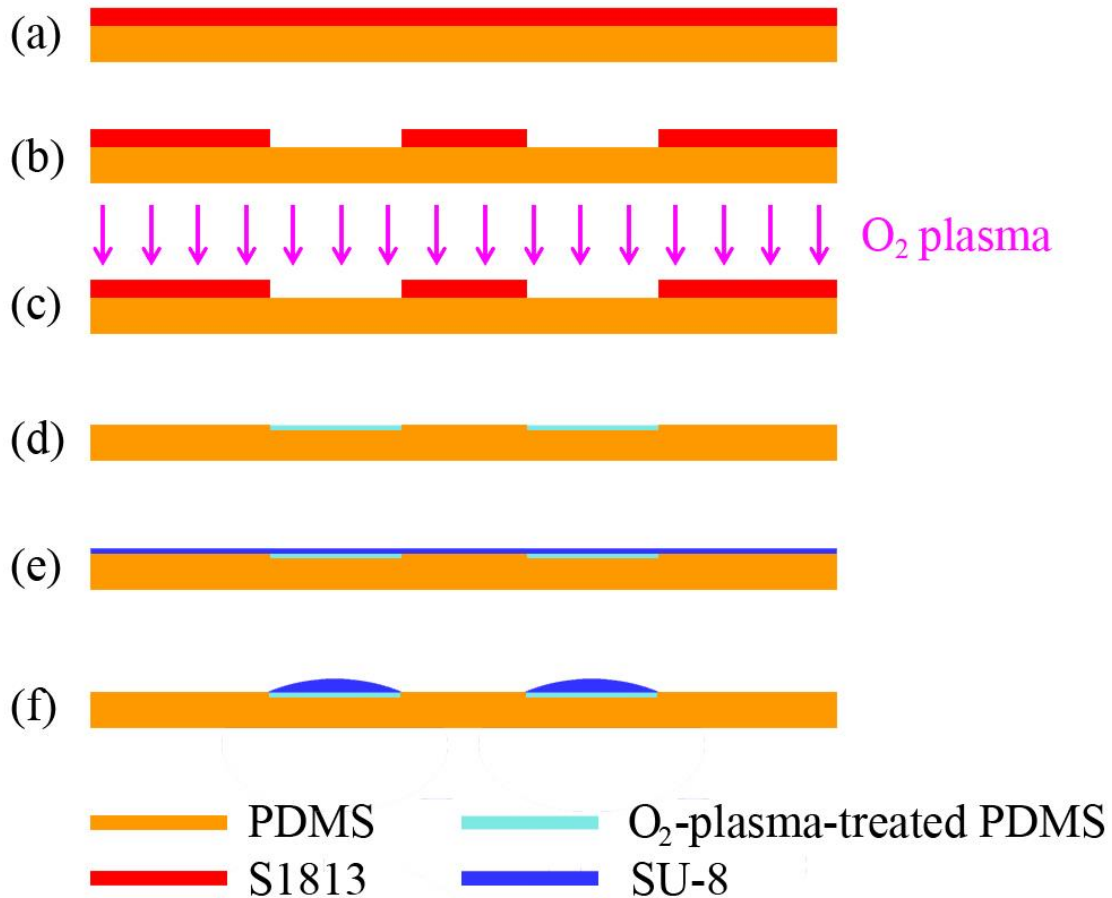


Figure 29 Process flow of SU-8 dewetting process on PDMS substrate.

The profile was measured by profilometer and shown in Figure 31, indicating the formation of spherical μ -lenses. The contact angle was estimated based on the μ -lens geometry and shown in Figure 32. After dewetting, SU-8 exhibits a contact angle of $\sim 30^\circ$ on the O₂-plasma-treated PDMS substrate, which shows a higher surface tension than the untreated surface, due to the introduction of new oxygen-related functional groups. Note that the diameters of μ -lenses are consistent with the dimension of the patterns treated by the O₂ plasma. Compared to thermal

reflow technology during which the micro-patterns could shrink, dewetting is much more convenient in producing μ -lens arrays with dimension easily controlled.

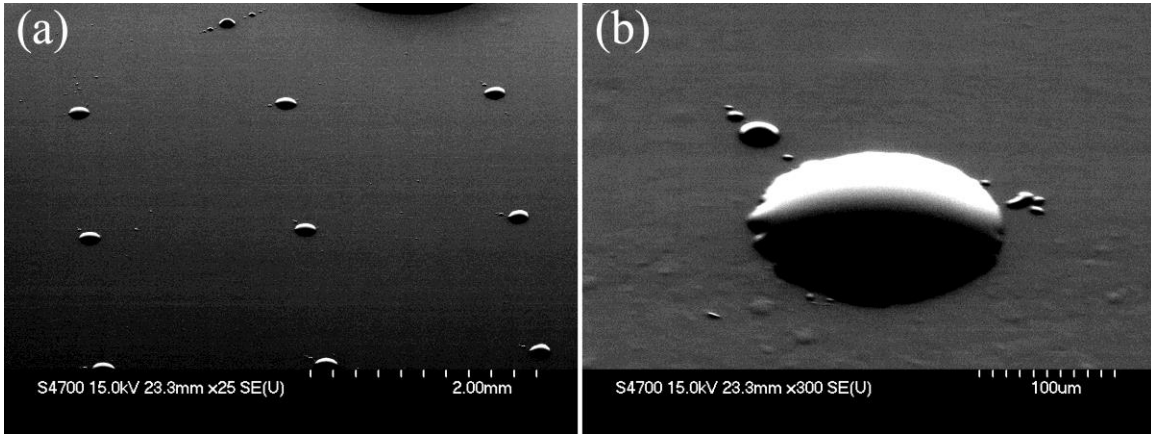


Figure 30 SEM images of (a) μ -lens array and (b) single μ -lens with an initial diameter of 200 μm after SU-8 dewetting on the PDMS substrate. Such array was self-organized onto the surface area that had been pre-treated by O_2 plasma.

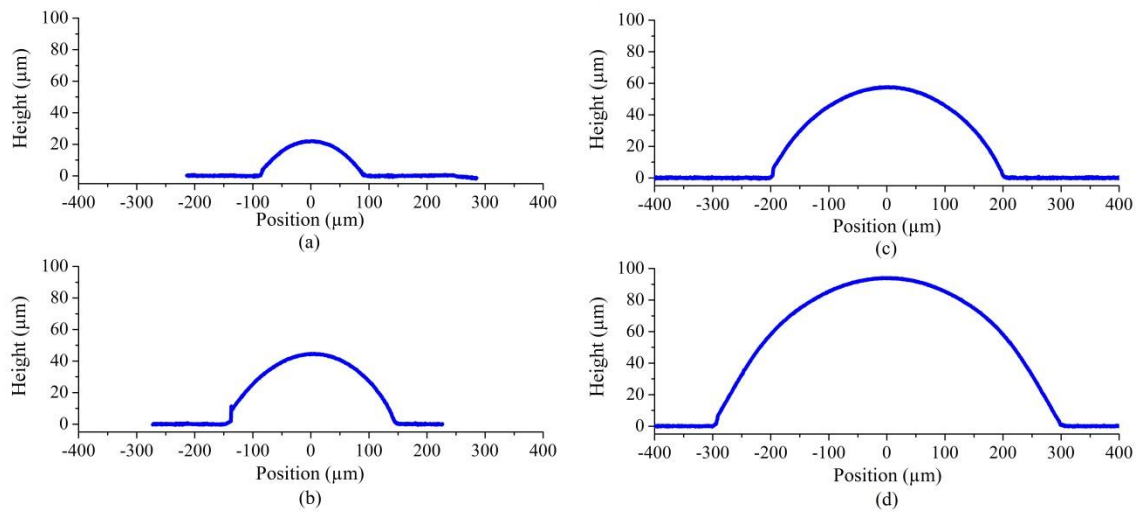


Figure 31 The profile of SU-8 μ -lenses with diameters of (a) 200 μm , (b) 300 μm , (c) 400 μm , and (d) 600 μm , which were fabricated by dewetting on pre-patterned PDMS substrates.

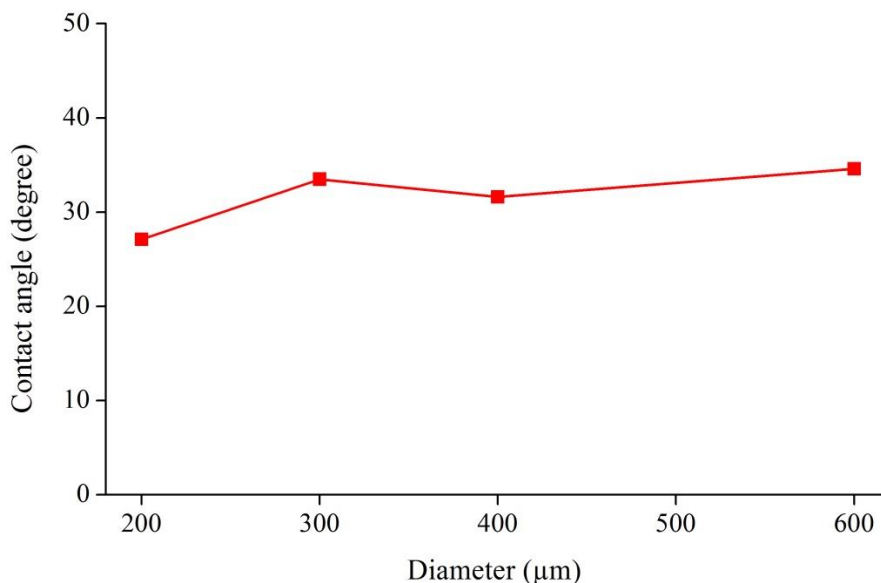


Figure 32 Contact angles of SU-8 μ -lenses with various diameters from 200 μm to 600 μm on the O_2 -plasma-treated PDMS substrate. The μ -lenses were fabricated by dewetting.

5.2.2 Room-temperature dewetting exploration

The possibility of occurrence of room-temperature dewetting has attracts a lot of attention because it benefits the integration of materials and components that cannot stand a high temperature. An approach of dewetting in the vapor atmosphere of the solvent of liquid polymer has been proposed. In our experiment, vapor of the SU-8 thinner (i.e., cyclopentanone) was used. After the spin-coating of SU-8 on PDMS which was patterned by O_2 plasma treatment in exactly the same way as previously, the substrate was placed into the vapor atmosphere of cyclopentanone. The dewetting occurred immediately and completed within 5 minutes, implying that the vapor of solvent can effectively lower the viscosity of SU-8 and increase its mobility, resulting in the glass transition at the room temperature.

5.2.3 Dewetting of SU-8 on Parylene-C

In order to achieve μ -lens arrays on flexible and biocompatible substrates, the dewetting experiment has been carried out on a Parylene-C thin film. The same process as on the PDMS substrate was attempted at first but dewetting did not take place, even if the substrate was baked up to 200 °C.

To increase the possibility of dewetting, SU-8 2000.2, another type of SU-8, was used for the following experiment. It is also the mixture of the same solute and solvent but with different proportion. A layer as thin as 200 nm can be obtained through spin-coating. In addition, the viscosity is also lowered due to a larger percentage of solvent, which is another advantage for the dewetting.

The contact angle of SU-8 2000.2 on the Parylene-C thin film was checked using a contact angle analysis system. It shows $\sim 0^\circ$, $\sim 0^\circ$ and 53.6° on the untreated, O₂-plasma-treated and SF₆-plasma-treated Parylene-C surfaces, respectively, which means the thin film of SU-8 2000.2 has a strong tendency to spread out on both the untreated and O₂-plasma-treated Parylene-C substrates. It explains why dewetting did not take place on the patterned Parylene-C substrate. On the other hand, the big difference between contact angles on O₂-plasma-treated Parylene-C and SF₆-plasma-treated Parylene-C can possibly provide a strong driving force to achieve the dewetting.

Consequently, the process was changed based on the discussion above. A brief process was performed for the proof-of-concept. 1 min SF₆ plasma treatment was first carried out on the whole Parylene-C substrate. After that the substrate was patterned by photolithography and the exposed area was treated by the O₂ plasma. After rinsing off the photoresist, SU-8 2000.2 was spin-coated on the surface. The sample was then transferred to the sealed environment with the

vapor atmosphere of cyclopentanone. The dewetting occurred immediately and finished within 3 minutes. Figure 33 shows the microscopic view of the surface before and after dewetting. The SU-8 μ -lens array with diameter of 120 μm can be clearly observed on the Parylene-C substrate after dewetting.

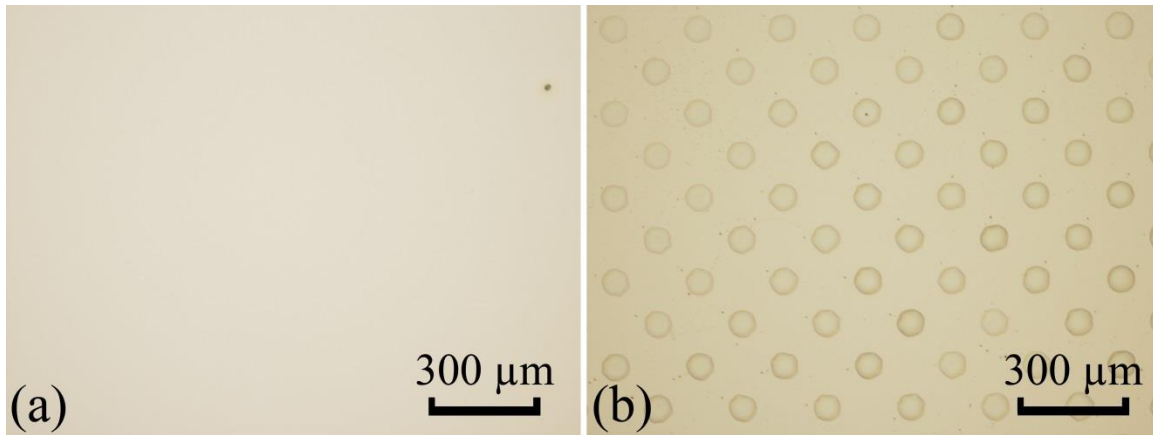


Figure 33 Microscopic view of the surface of (a) flat SU-8 coating on the Parylene-C substrate before dewetting; (b) SU-8 μ -lens array on the Parylene-C substrate after dewetting.

5.3 Summary

SU-8 μ -lens array has been successfully fabricated on both PDMS and Parylene-C substrates by the dewetting method, which is fast, low-cost, and most importantly, can occur at the room temperature. Viscosity, temperature and surface tension are the most important parameters that can influence the dewetting dynamics. The completion of dewetting on the Parylene-C thin film enables the fabrication of μ -lens array through dewetting on the flexible substrate. Further study on the theory of dewetting and characterization of formed μ -lenses will be done in the following work.

CHAPTER 6 Summary

A number of techniques, including soft lithography, surface tension modification, thermal reflow, and self-organized dewetting have been carried out to fabricate μ -lens arrays in order to improve the LED light out-coupling efficiency. 3-D printing and soft lithography were used to fabricate lenses with the classic design for large-scale LED lenses. The measurement in gelatin shows that the fabricated lenses help to collimate the LED light, but the low resolution due to the 3-D printing made this technique unfeasible in the micro scale. After that, surface tension driven methods have been explored to fabricate μ -lens arrays. The combined O_2 and SF_6 plasma treatments have been found to be effective in altering the surface wettability of polymers such as Parylene-C. Both super hydrophilicity and super hydrophobicity have been successfully achieved. However, polymer liquid cannot be dispensed accurately in the same way as water by syringe or pipette due to its high viscosity. Therefore, techniques of photoresist thermal reflow and self-organized dewetting have been studied to generate polymer-based μ -lenses. Thermal reflow is able to convert the photoresist cylinders into spherical cap-shaped lenses but high temperature is a drawback. Dewetting provides a simple, fast and self-organized method to fabricate μ -lens arrays by combining the surface tension modification technique. Especially the vapor atmosphere of the solvent enables the occurrence of dewetting at room temperature.

The main contributions of this thesis research are:

Contribution 1: Super hydrophobicity and super hydrophilicity have been achieved on Parylene-C films through fast and low-powered O_2 and SF_6 plasma treatments

The wettability of Parylene-C can be tuned through combined O_2 and SF_6 plasma treatments, which eliminates the need for designing complex micro- and/or nano-structures. This method is fast, simple and compatible with conventional microfabrication technology, and also can be

applied on both flat and curved surfaces.

Contribution 2: Developed a fast, self-organized, room-temperature dewetting method to fabricate polymer-based μ -lens arrays on chemically pre-patterned substrates.

The vapor atmosphere of cyclopentanone was proved to be effective in initializing the dewetting of SU-8 thin films at room temperature on chemically pre-patterned PDMS and Parylene-C substrates. Owing to the selective surface pre-patterning through SF₆ and O₂ plasma treatments, the dewetted droplets were self-organized to form μ -lens arrays. The dimension of lenses can be accurately controlled by the photomask.

REFERENCES

REFERENCES

- [1] A. Stroh and I. Diester, "Optogenetics: a new method for the causal analysis of neuronal networks in vivo," *Neuroforum*, vol. 18, no. 4, pp. 280-289, Nov. 2012.
- [2] E. S. Boyden, F. Zhang, E. Bamberg, G. Nagel, and K. Deisseroth, "Millisecond-timescale, genetically targeted optical control of neural activity," *Nature Neuroscience*, vol. 8, no. 9, pp. 1263-1268, Sep. 2005.
- [3] V. Gradinaru, F. Zhang, C. Ramakrishnan, J. Mattis, R. Prakash, I. Diester, *et al.*, "Molecular and cellular approaches for diversifying and extending optogenetics," *Cell*, vol. 141, no. 1, pp. 154-165, Apr. 2010.
- [4] M. Banghart, K. Borges, E. Isacoff, D. Trauner, and R. H. Kramer, "Light-activated ion channels for remote control of neuronal firing," *Nature Neuroscience*, vol. 7, no. 12, pp. 1381-1386, Dec. 2004.
- [5] K. Deisseroth, "Optogenetics," *Nature Methods*, vol. 8, no. 1, pp. 26-29, Jan. 2011.
- [6] P. Anikeeva, A. S. Andalman, I. Witten, M. Warden, I. Goshen, L. Grosenick, *et al.*, "Optetrode: a multichannel readout for optogenetic control in freely moving mice," *Nature Neuroscience*, vol. 15, no. 1, pp. 163-170, Jan. 2012.
- [7] J. J. Mancuso, J. Kim, S. Lee, S. Tsuda, N. B. H. Chow, and G. J. Augustine, "Optogenetic probing of functional brain circuitry," *Experimental Physiology*, vol. 96, no. 1, pp. 26-33, Jan. 2011.
- [8] F. Zhang, V. Gradinaru, A. R. Adamantidis, R. Durand, R. D. Airan, L. de Lecea, *et al.*, "Optogenetic interrogation of neural circuits: technology for probing mammalian brain structures," *Nature Protocols*, vol. 5, no. 3, pp. 439-456, Feb. 2010.
- [9] L. Buchen, "Neuroscience: Illuminating the brain," *Nature*, vol. 465, no. 7294, pp. 26-28, May 2010.
- [10] H. E. Covington, M. K. Lobo, I. Maze, V. Vialou, J. M. Hyman, S. Zaman, *et al.*, "Antidepressant effect of optogenetic stimulation of the medial prefrontal cortex," *Journal of Neuroscience*, vol. 30, no. 48, pp. 16082-16090, Dec. 2010.
- [11] A. V. Kravitz, B. S. Freeze, P. R. L. Parker, K. Kay, M. T. Thwin, K. Deisseroth, *et al.*, "Regulation of parkinsonian motor behaviours by optogenetic control of basal ganglia circuitry," *Nature*, vol. 466, no. 7306, pp. 622-626, Jul. 2010.
- [12] C. T. Wentz, J. G. Bernstein, P. Monahan, A. Guerra, A. Rodriguez, and E. S. Boyden, "A wirelessly powered and controlled device for optical neural control of freely-behaving animals," *Journal of Neural Engineering*, vol. 8, no. 4, pp. 046021-1–046021-10, Aug. 2011.

- [13] N. Grossman, V. Poher, M. S. Grubb, G. T. Kennedy, K. Nikolic, B. McGovern, *et al.*, "Multi-site optical excitation using ChR2 and micro-LED array," *Journal of Neural Engineering*, vol. 7, no. 1, pp. 016004-1–016004-13, Feb. 2010.
- [14] B. McGovern, R. B. Palmi, N. Grossman, E. M. Drakakis, V. Poher, M. A. A. Neil, *et al.*, "A new individually addressable micro-LED array for photogenetic neural stimulation," *IEEE Transactions on Biomedical Circuits and Systems*, vol. 4, no. 6, pp. 469-476, Dec. 2010.
- [15] P. Degenaar, B. McGovern, R. Berlinguer-Palmi, N. Vysokov, N. Grossman, V. Pohrer, *et al.*, "Individually addressable optoelectronic arrays for optogenetic neural stimulation," in *Proc. Int. Conf. BioCAS*, Nov. 2010, pp. 170-173.
- [16] K. Y. Kwon, A. Khomenko, M. Haq, and W. Li, "Integrated slanted microneedle-LED array for optogenetics," in *Proc. 35th Int. Conf. EMBC*, Jul. 2013, pp. 249-252.
- [17] A. M. Aravanis, L. P. Wang, F. Zhang, L. A. Meltzer, M. Z. Mogri, M. B. Schneider, *et al.*, "An optical neural interface: in vivo control of rodent motor cortex with integrated fiberoptic and optogenetic technology," *Journal of Neural Engineering*, vol. 4, no. 3, pp. S143-S156, Sep. 2007.
- [18] K. Y. Kwon, X. P. Bi, and W. Li, "Droplet backside exposure for making slanted SU-8 microneedles," in *Proc. 35th Int. Conf. EMBC*, Jul. 2013, pp. 767-770.
- [19] S. Moller and S. R. Forrest, "Improved light out-coupling in organic light emitting diodes employing ordered microlens arrays," *Journal of Applied Physics*, vol. 91, no. 5, pp. 3324-3327, Mar. 2002.
- [20] Y. Sun and S. R. Forrest, "Enhanced light out-coupling of organic light-emitting devices using embedded low-index grids," *Nature Photonics*, vol. 2, no. 8, pp. 483-487, Aug. 2008.
- [21] J. H. Lee, W. Chang, and D. Choi, "LED light coupler design for a ultra thin light guide," *Journal of the Optical Society of Korea*, vol. 11, no. 3, pp. 113-117, Sep. 2007.
- [22] J. J. Chen, T. Y. Wang, K. L. Huang, T. S. Liu, M. D. Tsai, and C. T. Lin, "Freeform lens design for LED collimating illumination," *Optics Express*, vol. 20, no. 10, pp. 10984-10995, May 2012.
- [23] <http://www.madeinasia.com/led-lens/>.
- [24] G. C. Shao, J. H. Wu, Z. L. Cai, and W. J. Wang, "Fabrication of elastomeric high-aspect-ratio microstructures using polydimethylsiloxane (PDMS) double casting technique," *Sensors and Actuators A-Physical*, vol. 178, pp. 230-236, May 2012.
- [25] H. B. Yu, G. Y. Zhou, F. S. Chau, and F. W. Lee, "Fabrication and characterization of PDMS microlenses based on elastomeric molding technology," *Optics Letters*, vol. 34, no. 21, pp. 3454-3456, Nov. 2009.
- [26] Y. H. Kang, S. S. Oh, Y. S. Kim, and C. G. Choi, "Fabrication of antireflection nanostructures by hybrid nano-patterning lithography," *Microelectronic Engineering*, vol. 87, no.

2, pp. 125-128, Feb. 2010.

[27] M. Holgado, C. A. Barrios, F. J. Ortega, F. J. Sanza, R. Casquel, M. F. Laguna, *et al.*, "Label-free biosensing by means of periodic lattices of high aspect ratio SU-8 nano-pillars," *Biosensors and Bioelectronics*, vol. 25, no. 12, pp. 2553-2558, Aug. 2010.

[28] B. P. Chaudhri, F. Ceyskens, P. De Moor, C. Van Hoof, and R. Puers, "A high aspect ratio SU-8 fabrication technique for hollow microneedles for transdermal drug delivery and blood extraction," *Journal of Micromechanics and Microengineering*, vol. 20, no. 6, pp. 064006-1–064006-6, Jun. 2010.

[29] L. Amato, S. S. Keller, A. Heiskanen, M. Dimaki, J. Emneus, A. Boisen, *et al.*, "Fabrication of high-aspect ratio SU-8 micropillar arrays," *Microelectronic Engineering*, vol. 98, pp. 483-487, Oct. 2012.

[30] E. Burkarter, C. K. Saul, F. Thomazi, N. C. Cruz, L. S. Roman, and W. H. Schreiner, "Superhydrophobic electrospayed PTFE," *Surface and Coatings Technology*, vol. 202, no. 1, pp. 194-198, Nov. 2007.

[31] R. N. Wenzel, "Resistance of solid surfaces to wetting by water," *Industrial and Engineering Chemistry*, vol. 28, no. 8, pp. 988-994, Aug. 1936.

[32] A. B. D. Cassie and S. Baxter, "Wettability of porous surfaces," *Transactions of the Faraday Society*, vol. 40, pp. 546-550, Sep. 1944.

[33] S. J. Zhu, Y. F. Li, J. H. Zhang, C. L. Lu, X. Dai, F. Jia, *et al.*, "Biomimetic polyimide nanotube arrays with slippery or sticky superhydrophobicity," *Journal of Colloid and Interface Science*, vol. 344, no. 2, pp. 541-546, Apr. 2010.

[34] K. K. S. Lau, J. Bico, K. B. K. Teo, M. Chhowalla, G. A. J. Amaratunga, W. I. Milne, *et al.*, "Superhydrophobic carbon nanotube forests," *Nano Letters*, vol. 3, no. 12, pp. 1701-1705, Dec. 2003.

[35] J. Yeo, M. J. Choi, and D. S. Kim, "Robust hydrophobic surfaces with various micropillar arrays," *Journal of Micromechanics and Microengineering*, vol. 20, no. 2, pp. 025028-1–025028-8, Feb. 2010.

[36] H. E. Jeong, S. H. Lee, J. K. Kim, and K. Y. Suh, "Nanoengineered multiscale hierarchical structures with tailored wetting properties," *Langmuir*, vol. 22, no. 4, pp. 1640-1645, Feb. 2006.

[37] Y. Yoon, D. W. Lee, and J. B. Lee, "Surface modified nano-patterned SU-8 pillar array optically transparent super-hydrophobic thin film," *Journal of Micromechanics and Microengineering*, vol. 22, no. 3, pp. 035012-1–035012-7, Mar. 2012.

[38] B. Lu, J. C. H. Lin, Z. Liu, Y. K. Lee, and Y. C. Tai, "Highly flexible, transparent and patternable parylene-C superhydrophobic films with high and low adhesion," in *Proc. 24th Int. Conf. MEMS*, Jan. 2011, pp. 1143-1146.

- [39] K. Tsougeni, N. Vourdas, A. Tserepi, E. Gogolides, and C. Cardinaud, "Mechanisms of oxygen plasma nanotexturing of organic polymer surfaces: from stable super hydrophilic to super hydrophobic surfaces," *Langmuir*, vol. 25, no. 19, pp. 11748-11759, Oct. 2009.
- [40] I. Woodward, W. C. E. Schofield, V. Roucoules, and J. P. S. Badyal, "Super-hydrophobic surfaces produced by plasma fluorination of polybutadiene films," *Langmuir*, vol. 19, no. 8, pp. 3432-3438, Apr. 2003.
- [41] E. C. Rangel, W. C. A. Bento, M. E. Kayama, W. H. Schreiner, and N. C. Cruz, "Enhancement of polymer hydrophobicity by SF₆ plasma treatment and argon plasma immersion ion implantation," *Surface and Interface Analysis*, vol. 35, no. 2, pp. 179-183, Feb. 2003.
- [42] M. Ataefard, S. Moradian, M. Mirabedini, M. Ebrahimi, and S. Asiaban, "Investigating the effect of power/time in the wettability of Ar and O₂ gas plasma-treated low-density polyethylene," *Progress in Organic Coatings*, vol. 64, no. 4, pp. 482-488, Mar. 2009.
- [43] W. Li, D. C. Rodger, E. Meng, J. D. Weiland, M. S. Humayun, and Y. C. Tai, "Flexible parylene packaged intraocular coil for retinal prostheses," in *Proc. Int. Conf. MMB*, May 2006, pp. 105-108.
- [44] P. Y. Li, J. Shih, R. Lo, S. Saati, R. Agrawal, M. S. Humayun, *et al.*, "An electrochemical intraocular drug delivery device," *Sensors and Actuators A-Physical*, vol. 143, no. 1, pp. 41-48, May 2008.
- [45] J. M. Hsu, L. Rieth, R. A. Normann, P. Tathireddy, and F. Solzbacher, "Encapsulation of an integrated neural interface device with parylene C," *IEEE Transactions on Biomedical Engineering*, vol. 56, no. 1, pp. 23-29, Jan. 2009.
- [46] S. Takeuchi, D. Ziegler, Y. Yoshida, K. Mabuchi, and T. Suzuki, "Parylene flexible neural probes integrated with microfluidic channels," *Lab on a Chip*, vol. 5, no. 5, pp. 519-523, May 2005.
- [47] X. Liu, L. Li, B. Awate, R. M. Worden, G. Reguera, and A. J. Mason, "Biosensor array microsystem on a CMOS amperometric readout chip," in *Proc. Int. Conf. BioCAS*, Nov. 2011, pp. 305-308.
- [48] J. S. Song, S. Lee, S. H. Jung, G. C. Cha, and M. S. Mun, "Improved biocompatibility of parylene-C films prepared by chemical vapor deposition and the subsequent plasma treatment," *Journal of Applied Polymer Science*, vol. 112, no. 6, pp. 3677-3685, Jun. 2009.
- [49] T. Trantidou, T. Prodromakis, and C. Toumazou, "Oxygen plasma induced hydrophilicity of parylene-C thin films," *Applied Surface Science*, vol. 261, pp. 43-51, Nov. 2012.
- [50] J. N. Chai, F. Z. Lu, B. M. Li, and D. Y. Kwok, "Wettability interpretation of oxygen plasma modified poly(methyl methacrylate)," *Langmuir*, vol. 20, no. 25, pp. 10919-10927, Dec. 2004.
- [51] K. S. Kim, K. H. Lee, K. Cho, and C. E. Park, "Surface modification of polysulfone

ultrafiltration membrane by oxygen plasma treatment," *Journal of Membrane Science*, vol. 199, no. 1-2, pp. 135-145, Apr. 2002.

[52] K. Tsougeni, P. S. Petrou, A. Tserepi, S. E. Kakabakos, and E. Gogolides, "Nanotexturing of poly(methyl methacrylate) polymer using plasma processes and applications in wetting control and protein adsorption," *Microelectronic Engineering*, vol. 86, no. 4-6, pp. 1424-1427, Apr./Jun. 2009.

[53] F. Walther, P. Davydovskaya, S. Zucher, M. Kaiser, H. Herberg, A. M. Gigler, *et al.*, "Stability of the hydrophilic behavior of oxygen plasma activated SU-8," *Journal of Micromechanics and Microengineering*, vol. 17, no. 3, pp. 524-531, Mar. 2007.

[54] J. F. Chang and H. Sirringhaus, "Patterning of solution-processed semiconducting polymers in high-mobility thin-film transistors by physical delamination," *Advanced Materials*, vol. 21, no. 24, pp. 2530-2535, Jun. 2009.

[55] K. Tsougeni, D. Papageorgiou, A. Tserepi, and E. Gogolides, ""Smart" polymeric microfluidics fabricated by plasma processing: controlled wetting, capillary filling and hydrophobic valving," *Lab on a Chip*, vol. 10, no. 4, pp. 462-469, 2010.

[56] P. Rezai, P. R. Selvaganapathy, and G. Rwohl, "Plasma enhanced bonding of polydimethylsiloxane with parylene and its optimization," *Journal of Micromechanics and Microengineering*, vol. 21, no. 6, pp. 065024-1-065024-13, Jun. 2011.

[57] M. Hudlický and A. E. Pavlath, *Chemistry of Organic Fluorine Compounds II: A Critical Review*, 1st ed. Washington, DC, USA: ACS, 1995.

[58] E. Chibowski, "Surface free energy of a solid from contact angle hysteresis," *Advances in Colloid and Interface Science*, vol. 103, no. 2, pp. 149-172, Apr. 2003.

[59] Z. D. Popovic, R. A. Sprague, and G. A. N. Connell, "Technique for monolithic fabrication of microlens arrays," *Applied Optics*, vol. 27, no. 7, pp. 1281-1284, Apr. 1988.

[60] http://www.microchemicals.eu/technical_information/reflow_photoresist.pdf.

[61] J. Lim, M. Jung, C. Joo, and S. Kang, "Development of micro-objective lens array for large field-of-view multi-optical probe confocal microscopy," *Journal of Micromechanics and Microengineering*, vol. 23, no. 6, pp. 065028-1-065028-7, Jun. 2013.

[62] H. H. Yang, C. K. Chao, M. K. Wei, and C. P. Lin, "High fill-factor microlens array mold insert fabrication using a thermal reflow process," *Journal of Micromechanics and Microengineering*, vol. 14, no. 8, pp. 1197-1204, Aug. 2004.

[63] E. Roy, B. Voisin, J. F. Gravel, R. Peytavi, D. Boudreau, and T. Veres, "Microlens array fabrication by enhanced thermal reflow process: Towards efficient collection of fluorescence light from microarrays," *Microelectronic Engineering*, vol. 86, no. 11, pp. 2255-2261, Nov. 2009.

[64] H. Yang, C. K. Chao, C. P. Lin, and S. C. Shen, "Micro-ball lens array modeling and

fabrication using thermal reflow in two polymer layers," *Journal of Micromechanics and Microengineering*, vol. 14, no. 2, pp. 277-282, Feb. 2004.